GL03855-B

THE PETROLOGY OF THE APOLLO 12 ILMENITE BASALT SUITE

Michael A. Dungan
NRC-Resident Research Associate
NASA Johnson Space Center
Houston, Texas 77058

and

Roy W. Brown
Lockheed Electronics Company, Inc.
Houston, Texas 77058

Submitted to Proceedings of the 8th Lunar Science Conference

April 26, 1977

Abstract

The Apollo 12 ilmenite basalt suite encompasses the range of variation in cooling history and chemical differentiation observed in low-titanium mare basalts. Numerous consistencies have emerged in the integration of combined mineral chemistry data and petrographic interpretations with fractionation modeling determined independently on the basis of bulk chemistry. The major conclusion we have derived from this petrologic synthesis is that the bulk chemical variations in the ilmenite suite can be reconciled with differentiation within a single cooling unit. The critical observation is that included within the suite there are (1) olivine porphyritic basalts, (2) medium-grained basalts with evolved compositions and (3) coarse-grained olivine cumulates. Most of the chemical variation within the suite can be accounted for by fractionation of olivine equivalent to the composition of phenocrysts in vitrophyre 12008 which serves well as a parental magma for the other textural-chemical variants.

We have determined the relative cooling rate sequence within all three textural-chemical subgroups and found that mineral chemistry variations dependent on cooling rate (e.g., pyroxene compositions, spinel parageneses and mineral re-equilibration) are entirely consistent with this order. Furthermore, there are systematic correlations between the degree of olivine addition or subtraction and the relative cooling rate. The descending cooling rate sequence among the rapidly chilled porphyritic basalts corresponds to slightly increasing olivine removal. They are, therefore, believed to be represenative of the cap of the flow. The medium-grained basalts include members with compositions indicative of variable degrees of olivine fractionation, with progressive removal correlating positively with increasing cooling rate. The cumulates represent the complementary derivatives of the evolved basalts and must underlie them in the stratigraphic sequence.

I. Introduction

During the initial study of the Apollo 12 basalts, four magmatic groups were recognized on the basis of modal mineralogy and bulk chemistry. Several samples characterized by relatively high TiO_2, FeO and low SiO_2 plus correspondingly abundant ilmenite were classified as the "ilmenite suite" basalts (ISB). Although the samples that are presently recognized as members of this group differ in part from earlier classifications (e.g., Warner, 1971; James and Wright, 1972) the general scheme remains valid and the terminology has been retained.

The Apollo 12 ilmenite basalts were the least well-characterized cogenetic group of mare basalts in the lunar sample collection prior to the current re-examination of the Apollo 12 basalts by an informal JSC consortium (Rhodes et al., 1977, Nyquist et al., 1977 and Gibson et al., 1977). Some of the major results of these collaborative studies are that (1) the ilmenite suite basalts have been shown to comprise a significant proportion of the samples collected at the site and are, therefore, probably indigenous to it, (2) the compositional range of the ISBs extends from very magnesian cumulates to evolved quartz-normative basalts and (3) they have been shown to be distinct from the other two major Apollo 12 basalt types, the olivine and pigeonite groups, on the basis of both major and trace elements (Rhodes et al., 1977) and $^{87}Sr/^{86}Sr$ initial ratio (Nyquist et al., 1977).

We have studied five key samples from the Apollo 12 ilmenite basalt suite (12008,20; 12045,6; 12056,7; 12016,14 and ,18; 12005,13) of varying petrography and bulk chemistry, reviewed the literature for available information on other well-studied samples and examined thin sections of all the samples in this suite. The purpose of the study has been to relate variations in texture, modal mineralogy and mineral chemistry among these samples to variations in post-eruption crystallization history.

II. Analytical Techniques

Microprobe analyses of spinels in 12005 and all reported analyses for plagioclase, olivine and metal were performed on an A.R.L., EMX-SM electron microprobe using mineral and pure element standards at 15KV acceleration potential and 20 nanoamperes sample current on clinopyroxene. Raw data were processed on a PDP 1120 computer for dead time, instrumental drift, background and matrix corrections (Bence-Albee method for silicates and spinels). Matrix corrections for metal data were obtained using a version of the Mason and Frost program (MK5).

Zoned pyroxene, spinel and ilmenite in samples 12045, 12008, 12016, 12005 and 12056 were analyzed on an automated (stage and spectrometers) M.A.C. 5 electron microprobe. Operating conditions were 15KV acceleration potential and 40 nanoamperes sample current on benitoite. Mineral standards were used throughout the analysis. Raw data were corrected for dead time, background, and matrix corrected using a Bence-Albee routine. Structural formulae and relevant cation and oxide ratios for each sample point are printed out on line.

Modal analyses were accomplished on the automated M.A.C.5 electron microprobe using a count rate-dependent sieving technique keyed to certain elements. Data are taken on an orthogonal grid with pre-determined point spacings using a sharply focused beam. A minimum of 2000 data points were classified during modal analysis. Initially spectrometers are set for a "silicate loop" (Fe, Ca, Si). If the count rate permits classification of the data point as either olivine, plagioclase, low-Ca pyroxene, high-Ca pyroxene, or phosphate, the stage then moves to the next data point. If none of these phases can be identified, then depending on the count rate for Si a "K-loop" or "oxide-loop" or others #1 is chosen. K-loop-Si and K are set on #2 and #3 spectrometers respectively, classification is attempted as Si-rich mesostasis, silica phase or

K-feldspar. In the oxide loop spectrometers #1 and #2 are set on Fe and Ti respectively. Classification of the point as metal, troilite, spinel, ulvöspinel, ilmenite, armalcolite or rutile is attempted. Points which cannot be classified as such are classified as others and are not used in the mode computation.

III. Petrography

12008 - This sample is the most fine-grained and rapidly quenched of the porphyritic ISBs and is very similar in textures and mineralogy to the Apollo 12 olivine suite vitrophyres 12009 and 12015 (Figure 1a, b). The liquidus phase, olivine, is represented by ≈15-20% equant subhedral to euhedral phenocrysts (0.2 - 0.5 mm) heterogeneously distributed in the groundmass as glomerophyric aggregates. The most magnesian phenocryst core composition measured is Fo_{72} but most are Fo_{71-68} with narrow rims of Fo_{67-56}. Titanian chromian spinel is the second phase to crystallize. It occurs as small idiomorphic octahedra (0.01 - 0.05 mm) and as glomerophyric aggregates in the groundmass or as inclusions in the rims of olivine phenocrysts. Spherical metal droplets are typically associated with the spinel as inclusions or attached to grain margins. More rarely they are found as inclusions in olivine. Spherical melt inclusions are abundant in the cores of olivine phenocrysts in 12008 and in all the other samples studied.

A second generation of olivine is present as skeletal microphenocrysts in the groundmass and as ornamental overgrowths on the early equant grains. The dominant morphology of the second generation is chain-like (Donaldson, 1976). The composition of these grains is the same as the phenocryst rims. Individual "chains" are up to 0.5 mm long and are typically 0.02 - 0.03 mm in width. The skeletal olvine precedes pyroxene, plagioclase and ilmenite in the crystallization sequence. Olivine crystallization terminated at the appearance of these groundmass phases. Groundmass metal and troilite are also absent.

The first groundmass phase is aluminous titanaugite in the form of feathery dendritic crystals up to 0.5 mm across. Only a few of the dendrites in the section examined are coarse enough for microprobe analysis. Most merge with the extremely fine-grained to cryptocrystalline matrix consisting of ilmenite (less than 1 μm) and a silicate phase of lower reflectivity than pyroxene (plagioclase?). Ilmenite occurs as groups of sub-parallel wispy filaments and as tiny, scattered equant cruciform grains.

12045 - As in 12008, the early phenocryst phases are glomerophyric aggregates of equant olivine phenocrysts, spinel grains and rare metal droplets. The chemistry of these phases is essentially identical to those in 12008 with the exception of the spinel which is zoned to ulvöspinel rims in 12045. This zoning only occurs on spinel grains not enclosed in olivine phenocrysts. Ulvöspinel microphenocrysts (some skeletal) are also present in the groundmass. The second generation of olivine in 12045 is less skeletal than in 12008. It generally forms ornamental overgrowths on phenocrysts in the form of acicular appendages.

Unlike 12008 the early pyroxene occurs as elongate non-skeletal phenocrysts and rims on olivine phenocrysts. They are zoned, brown titanaugite similar in composition to those in 12008. The phenocrysts are cigar-shaped grains which typically cluster in subparallel aggregates. The augite, spinel and olivine phenocrysts are set in a variolitic groundmass of acicular pyroxene, plagioclase (An_{93-84}), a silica phase, ilmenite, troilite and metal. The ilmenite is highly skeletal and occurs as parallel sets of thin platelets (0.2 - 0.7 mm x 10 μm) spaced at roughly 50 μm intervals. The parallelism of the individual platelets apparently reflects the presence of large framework grains that nucleated epitaxially on early pyroxene. Ilmenite appears to be the first groundmass phase to crystallize (Figure 1c, d).

12022 - Porphyritic basalts 12045 and 12022 are fundamentally similar in textures, mineralogy, mineral chemistry and bulk composition (Weill et al., 1971; see their Figure 2). A less rapid cooling rate for 12022 is indicated by a coarsening of all the groundmass phases. Pyroxene phenocrysts in particular are larger and less elongate. Their compositions also vary in a way consistent with growth at lesser undercooling than in 12045 (see below).

12056 - Sample 12056 is a medium-grained microgabbro with a seriate subophitic texture (Figure 2d). The crystallization sequence is olivine, metal and chromian spinel, followed by pyroxene in a peritectic reaction-relationship with olivine, ulvöspinel, plagioclase, ilmenite and mesostasis consisting of a silica phase, Si + K-rich glass, fayalite, phosphate, metal and troilite.

Olivine is less abundant (Table 2) than in the porphyritic basalts (Dence et al., 1971) and generally occurs as rounded, partly resorbed inclusions in larger pyroxenes. Small olivine grains included in plagioclase are subhedral rather than rounded and embayed. The rock is dominated modally by pyroxene. The cores of large grains are predominantly augite with minor intergrown low-calcium pyroxene. These larger grains tend to be elongate (1.0 - 1.5 mm by 0.3 - 0.6 mm). Textural evidence coupled with microprobe data indicate that the rims of these large grains and the finer-grained pyroxene in 12056 co-crystallized with plagioclase, ilmenite and ulvöspinel. It is this phase of crystallization that gives rise to the subophitic texture and graphic intergrowths of plagioclase and pyroxene. Plagioclase morphology varies from equant to highly elongate. Early, equant plagioclase (0.3 - 0.5 mm) contains inclusions of pyroxene indicative of formation as a cored grains, suggesting nucleation at substantial undercooling. The larger plagioclase laths, which are also in part cored, are up to 0.7 mm in length. Most of the lath-shaped grains range in length from 0.4 to 0.2 mm and are 0.05 - 0.2 mm wide. Ilmenite morphology is generally elongate. Ilmenite also tends to be skeletal and contain abundant silicate inclusions. Subsolidus reduction assemblages replacing ilmenite and ulvöspinel are rare.

12056 contains several percent of segregations of late-stage mesostasis which consist primarily of crystalline phases intimately intergrown in a symplectoid texture with minor Si + K-rich glass. The dominant phase is fayalitic olivine in which spheroidal blebs of the alkali-rich glass are included. The textural relationships between fayalite and the Si + K-rich glass are interpreted as evidence of immiscibility in the residual liquid. The phosphate is generally dispersed throughout as small elongate to acicular grains (≈10 μm) whereas the silica phase occurs as a few anhedral interstitial grains intergrown with fayalite and the surrounding plagioclase and ferroaugite (Figure 2e, f). Ilmenite, metal and troilite are also invariably present in the mesostasis. Crystallization of the mesostasis into discrete phases with only the Si + K glass remaining is characteristic of most of the other evolved ISBs (e.g., 12051 - Keil et al., 1971; 12063 - El Goresy et al., 1971).

12051, 12054, 12047 and 12063: These four basalts are similar in petrography and modal mineralogy to each other and to 12056. They differ from 12056 in that they contain substantially less modal olivine. Olivine is absent in 12051 (Keil et al., 1971; Busche et al., 1972),12054 (Schaal and Horz, 1977) and 12047 with the exception of fayalite in the mesostasis. These three samples are chemically more evolved than 12056 and 12063 and contain substantial normative and modal silica (Rhodes et al., 1977). The textures are medium-grained, equigranular-ophitic: lath-shaped plagioclase and equant to slightly elongate pyroxenes form an intergrowth suggestive of cotectic crystallization. The morphology of plagioclase tends to be highly elongate laths and differs significantly from 12056 and 12016 which contain more equant plagioclase. Elongate ilmenite crystals are a significant phase (up to 9%). Small segregations of symplectoid mesostasis consisting of fayalite, silica, Si + K-rich glass, phosphate and alkali feldspar are dispersed

throughout. On the basis of plagioclase morphology and dimensions 12051, 12047 and 12054 are judged to have had more rapid cooling histories than 12063 and 12056.

12016 - This is an equigranular, medium-grained microgabbro (Figure 2a). In its mineralogy, textures, grain size and sequence of crystallization it is essentially similar to 12056. However, the non-evolved bulk chemistry of 12016 is matched by modal differences (less ilmenite, more olivine) and textural relationships differ in such a way as to suggest a slower cooling history.

Olivine in 12016 occurs as resorbed grains within pyroxenes and as subhedral to euhedral grains enclosed in plagioclase. One olivine grain is substantially larger (1.2 mm) than others in the rock or in the porphyritic basalts. Pyroxenes tend to be elongate but more equant and less seriate than in 12056 (0.5 - 1.0 mm). The pyroxenes are complex intergrowths of augite and low-calcium pyroxene although augite dominates the cores. Unlike the chemically evolved ISBs, equant plagioclase dominates over lath-shaped grains. Ophitic texture is poorly developed. Rather, plagioclase occurs interstitially to segregations of pyroxene grains and partly resorbed olivine. Where plagioclase occurs as large branching grains, a sub-poikilitic textures is developed. Ilmenite morphology is variable, including both highly elongate and equant grains (0.5 mm). However, compared to 12056, those in 12016 are more equant, less skeletal and tend also to be subpoikilitic.

The mesostasis textures in 12016 differ substantially from those in 12056. Figure 2c, d illustrate an anomalously large mesostasis segregation containing the same phases present in 12056, 12051, etc. The symplectoid texture is notably absent. Instead there are grains of fayalite, silica and phosphate in a crypto-crystalline matrix which appears to consist of devitrified glasses of contrasting composition similar to those expected from immiscibility. Textural relations indicative of immiscibility are absent.

12005 - This rock is heterogeneous, consisting of two distinct textural-mineralogical domains (Figure 3). Large pyroxene oikocrysts (2 - 6 mm) enclose an early crystallizing assemblage of rounded and embayed olivine (Figure 4c, d), single grains and glomerophyric aggregates of spinel and minor associated metal. Pyroxene oikocrysts are bounded by narrow bands of an interstitial assemblage dominated by euhedral to subhedral olivine grains poikilitically enclosed in plagioclase. Scattered throughout the interstitial areas are irregular branching ilmenites that poikilitically enclose olivine and pyroxene. Additional phases are augite and low-calcium pyroxene, ulvöspinel, smaller euhedral grains of ilmenite and minor holocrystalline mesostasis segregations consisting of plagioclase, K-feldspar, phosphate, ilmenite, troilite and metal.

The duality of olivine textures present in 12056 and 12016 is rampant in 12005. The contrast between the textures and modal amount of olivine within pyroxene oikocrysts and those in the interstitial area is striking (Figure 3, 4a, 4c). Extensive resorption of olivine in the early stages of crystallization is indicated. Several of the isolated anhedral olivine grains within the oikocrysts are in optical continuity with neighboring grains suggesting 80% resorption of >1 mm olivines. There is a single very large olivine interstitial to several pyroxene oikocrysts which is embayed and irregular in outline but is still 3 mm in diameter (Figure 3, 4d). It is in optical continuity with another isolated olivine implying an original diameter of >5 mm. The embayed grains within pyroxene are more magnesian (Fo_{66-60}) than the euhedral to subhedral grains intergrown with plagioclase (Fo_{61-57}).

Pyroxene oikocrysts are composite, with cores consisting primarily of augite and rims dominated by low-calcium pyroxene. However, intergrowths of low-calcium pyroxene are present in the cores of some oikocrysts, particularly as partial rims on rounded and embayed olivine. This relationship suggests that low-calcium

pyroxene was formed initially in the peritectic reaction-relatioship responsible for olivine resorption and the growth of the large oikocrysts. Subsequently augite became the dominant phase. The core-rim transition to low-calcium pyroxene probably reflects the incoming of plagioclase and ilmenite as pyroxenes intimately intergrown with plagioclase are compositionally similar to the rims. Rim augite occurs only in the outermost margins of the oikocrysts. Both cores and rims contain microscopic exsolution lamellae that were not resolvable with the microprobe. A mineral orientation fabric is imparted to 12005 by the parallelism of the long dimensions of the pyroxene oikocrysts.

Lath-shaped plagioclase is very rare, the dominant morphologies being equant (0.5 mm) and large poikilitic grains (Figure 4a, b). Plagioclase is intergrown with pyroxene oikocrysts only at their outermost margins. Similarly, ilmenite is present within the pyroxene oikocrysts only as a phase in crystallized melt inclusions and in the rims. Within the interstitial assemblage, ilmenite is present in two distinct habits. Prominent irregular, branching ilmenites (up to 1 mm) poikilitically enclose olivine and pyroxene (Figure 4f). Smaller grains lacking any included phases are generally idiomorphic and are equant to slightly elongate.

The modal amount, mineralogy and textures of mesostasis segregations in 12005 contrast with those in 12056 and 12016. Mesostasis phases constitute less than 0.5 percent of the mode in 12005. Both a silica phase and strongly iron-enriched ferromagnesian minerals are lacking. Instead the holocrystalline intergrowths consist of relatively sodic plagioclase (An_{73}), K-feldspar and phosphate plus ilmenite, metal and troilite (Figure 5). Thus, the only phases restricted to the mesostasis (K-feldspar and phosphate) are those minerals whose composition includes as an essential component elements that cannot be incorporated into the major constituent phases. Where present, mesostasis segregations are typically trapped between pyroxene oikocrysts or in embayments in the large poikilitic ilmenites.

Subsolidus reduction in ilmenite and ulvöspinel is widespread in 12005. Most ulvöspinel grains contain ilmenite lamellae and ilmenite grains in contact with mesostasis segregations contain rutile + chromian spinels (Figure 5). Small veinlets of metal, typically associated with troilite, cut silicates and oxide phases.

12036 - Sample 12036 exhibits the same type of textural-mineralogical heterogeneity as 12005. Pyroxene oikocrysts (5 mm) tend to be more equant than in 12005 and contain less olivine as chadacrysts. Textural relations in the interstitial assemblage are similar to those in 12005. Keil et al. (1971) and Busche et al. (1971) provide additional petrographic details and mineral chemistry data.

IV. Fractionation - Crystallization Model for the Ilmenite Suite Basalts

Integration of petrographic, modal (Tables 1 and 2) and phase chemical data in this study with major, minor and trace element analyses of Rhodes et al. (1977) and Nyquist et al. (1977) provides a basis for modeling of petrologic interrelationships among the demonstrably cogenetic ISBs. The eleven ISB samples have been ranked (from top to bottom in Table 1) in order of decreasing cooling rate on the basis of textural criteria; particularly plagioclase dimensions (cf., Walker et al., 1976b). This study is primarily concerned with relating the petrography and phase chemistry of the individual samples to the dependent variables cooling history, fractionation history and bulk chemistry. The basic petrologic framework for the discussion of mineral chemistry data which follows is summarized below.

1. Papike et al. (1976) and others have noted the paucity of mare basalts with Fe/(Fe+Mg) = 0.49 - 0.50 and suggested that this is a fundamental characteristic of unfractionated partial melts; the bimodal distribution of compositions at higher and lower Fe/(Fe+Mg) being complementary derivatives produced by near surface crystal fractionation of the rarely sampled parental liquids. Olivine-porphyritic

basalts with Fe/(Fe+Mg) = 0.51 - 0.49 are relatively abundant at the Apollo 12 site and serve well as parental magmas for fractionation modeling of the evolved basalts and olivine cumulates.

The best available candidates for basalts of a composition that could be parental to derivatives in the ilmenite and olivine basalt suites are the vitrophyres 12008 and 12009-12015 respectively, as the extremely rapidly chilled groundmasses of these rocks suggest minimal redistribution of phenocrysts subsequent to eruption. They are distinguished chemically by higher TiO_2 in 12008 and different trace element signatures, but in terms of major element characteristics (e.g., Fe/(Mg+Fe): 12008 = 0.50, 12015 = 0.49) they are fundamentally alike. Similar crystallization histories are also indicated by the fact that all three vitrophyres contain ≈15% equant olivine phenocrysts in a quenched groundmass that also includes some skeletal olivine. Experimental calibration of cooling rate dependent olivine morphologies in a synthetic 12009 composition led Donaldson et al. (1975) to conclude that the early equant olivine phenocrysts grew during relatively slow pre-eruption cooling at rates of 1° - 9° C/hr in contrast to the much more rapidly chilled groundmass (40° - 100° C/hr). The compositional and textural similarities of 12008 and 12009 indicate to us that their crystallization histories must have been very similar and the major results (if not absolute cooling rate values) of the cooling rate experiments on 12009 can be extrapolated to 12008. The recognition of a two-stage cooling history is a very important step in interpreting the details of olivine fractionation in the ISBs. The major implication is that the magma parental to the fractionated ISBs was erupted at 80 - 100°C below its liquidus containing ≈15 percent olivine phenocrysts which grew at comparatively slow cooling rates over a wide temperature range. The availability of olivine phenocrysts for fractionation is important in light of calculations by Rhodes et al. (1977) that demonstrate that chemical variations within the two groups can be

largely accounted for by addition or subtraction of olivine equivalent to the average composition of phenocrysts in the vitrophyres. This implies that in coarse-grained rocks, olivine fractionation took place very early in the post-eruption cooling history.

Only very rapidly cooled portions of the eruptive unit, represented by the vitrophyres did not fractionate abundant olivine. Groundmass textures in all three basalts are indicative of formation at substantial undercooling with the decreasing cooling rate sequence being 12008→12045→12022. The somewhat more slowly cooled porphyritic basalts 12022 and 12045 are slightly more evolved in composition (seven percent and two percent olivine removal respectively) than 12008. Thus, the settling velocity of olivine was great enough that phenocrysts were lost from the cooling regime that gave rise to a variolitic groundmass texture. Olivine accumulation in rapidly cooled olivine basalts 12075, 12076 and 12004 (Walker et al., 1976b; Rhodes et al., 1977) is likewise indicative of the mobility of olivine phenocrysts in these low-viscosity magmas (Weill et al., 1971; Table 2). As Walker et al. (1976b) have shown, the modal and normative olivine-contents in these rocks agree quite closely (particularly for rapidly cooled samples). This provides an additional petrographic check on the fractionation model (see Table 2).

2. The medium-grained, equigranular basalts are presumed to have formed under the chilled carapace of porphyritic basalts. They are characterized by non-porphyritic textures indicative of cooling rate histories intermediate between the porphyritic basalts and cumulates. There is an inverse correlation between cooling rate and percentage of modal olivine within this group. Samples 12051, 12054 and 12047, which are the most chemically evolved of the suite, lack normative and modal olivine (except for fayalite in the mesostasis) and exhibit textural relations suggestive of cotectic plagioclase and pyroxene crystallization. These textural-chemical relations indicate that olivine phenocrysts were removed completely from this section of the flow before pyroxene crystallization commenced. Modal and

normative data agree quite well for each rock and with the proposition that the bulk compositions of 12051, 12054 and 12047 represent removal of about 15 percent olivine phenocrysts from the parental basalt. The less evolved members of this subgroup, 12063 and 12056, contain modal and normative olivine and are characterized by textural relations indicative of less rapid cooling histories. Stratigraphically these are placed below 12054, 12047 and 12051, near the lower level of the zone from which there was a net loss of olivine phenocrysts.

The medium-grained basalt 12016 has a major element bulk composition quite similar to the porphyritic basalts. Based on textural criteria, its position in the cooling rate sequence must be somewhere between the evolved sample 12056 and the cumulates 12036 and 12005. Thus, the stratigraphic position of 12016 is presumed to be at the level in the flow where the gain of olivine from above compensated for the loss by settling.

3. Samples 12036 (Keil et al., 1971; Busche et al., 1972) and 12005 are the complementary cumulus derivatives of the evolved medium-grained basalts. Consequently their stratigraphic positions must have been below the evolved samples. The normative olivine content of 12005 (42%) is about 2.5 times the amount in the parental basalt,in agreement with modeling calculations that suggest approximately 30 percent olivine accumulation relative to 12008. Rhodes et al. (1977) have shown, however, that the differentiation is more complex than simple olivine fractionation. Calculation of the fractionation on the basis of major elements does not agree in detail with models derived from application of partition coefficient data and magmaphile element concentrations (Ti, Ba, K, P and REE). The cumulates are depleted in these elements relative to the values expected from simple olivine accumulation. Selective loss of the magmaphile elements by isothermal diffusion into the overlying liquid is supported by (1) the paucity of mesostasis phases enriched in the magmaphile elements, (2) the notable lack of iron enrichment in the ferromagnesian minerals and (3) the large pyroxene oikocrysts, formed by adcumulus growth, that modally dominate the two samples.

V. Mineral Chemistry

Olivine

Olivine is clearly the liquidus phase in the porphyritic ISBs. This was shown experimentally by Green et al. (1971) in one atmosphere phase equilibria studies of 12022. Olivine crystallizes alone to 100°C below the liquidus where it is joined by spinel at 1200°C and then pyroxene, plagioclase and ilmenite in the interval 1150° - 1125°C. The equilibrium liquidus olivine composition in these experiments is Fo_{77}. Weill et al. (1971) report olivine compositions in the range Fo_{76-58} in 12022. Butler (1972) found phenocryst cores in 12022 of Fo_{70-74} and Fo_{73} in 12008. The maximum Fo-contents of olivines in 12045 and 12008 analyzed in this study are Fo_{74} and Fo_{72} respectively. Most of the olivine core compositions measured in this study and by Butler fall in the range $Fo_{71.5-69.5}$. Thus, the most magnesian core composition analyzed among the three rocks occurs in the most evolved sample, 12022. The sample with the lowest maximum Fo-content is 12008 and 12045 is intermediate in terms of its bulk composition and the maximum Fo-content of its phenocrystic olivine. The cores of the olivine phenocrysts are broad and weakly zoned. Sharply zoned rims, in which spinel octahedra are included, range in composition (in all three porphyritic basalts) from Fo_{67-65} to Fo_{60-54}. We concur with Butler (1972) that reequilibration between early formed phenocryst cores and residual liquid has not substantially modified them and is, therefore, not responsible for olivine less magnesian than the experimental liquidus composition. These more iron-rich olivines are probably the result of crystallization over the 100°C temperature interval prior to the incoming of spinel (Green et al., 1971).

The rims of olivine phenocrysts and skeletal microphenocrysts are essentially equivalent in composition to each other within and among the three porphyritic basalts (Fo_{67-54}). The termination of olivine crystallization occurs approximately

at the incoming of the first pyroxene, as demonstrated by epitaxial overgrowths of augite on olivine phenocrysts in 12045 and 12022. Weill et al. (1971) suggested by a phenomenon observed in experimentally produced feldspar intergrowths (Lofgren and Gooley, 1977), is that on rapid post-eruption cooling a substantial boundary diffusion layer formed around the olivine phenocrysts resulting in enhanced pyroxene nucleation.

The rounded and embayed morphology of olivine included in large pyroxene grains in 12056, 12016 and 12005 is evidence for a peritectic reaction-relationship. However, there is a duality of olivine textures in these rocks in that olivine surrounded by plagioclase tends to be euhedral to subhedral and exhibit no evidence of reaction. Moreover, the range of olivine compositions in 12056 and 12016 extends from Fo_{73} to Fo_5 and Fo_{67} to Fo_7 respectively. Among the three samples 12056, 12016 and 12005 there is an inverse relationship between Mg/(Mg+Fe) in the bulk rock and the most magnesian olivine analyzed (Figure 6). However, there is a positive correlation between maximum Fo-content and the cooling rate sequence (Table 1) determined on the basis of textural criteria. This trend apparently reflects the cooling rate-dependence of reequilibration (Moore and Evans, 1967). Similar compositional and textural patterns are present in the Apollo 12 olivine basalts (Walker et al., 1976). The olivines in 12016 and 12005 have much lower Cr_2O_3 at a given Fo-content than those in the porphyritic basalts or even 12056 (Figure 6). The lower chromium in olivine of the more slowly cooled rocks is also ascribed to reequilibration. The cores of the largest grains and those completely enclosed in pyroxene are the most magnesian in a given rock. Zoning in these mantled grains is limited to ≈5% Fo whereas olivines which remained in contact with residual liquid exhibit much larger compositional differences between core and rim as well as asymmetric zoning in partially enclosed olivine.

On the basis of contrasting chromium and titanium concentrations in olivine from 12009-12004 and 12008-12022,Butler (1972) inferred two distinct Apollo 12 magma groups (for essentially texturally identical samples) that have now been proven valid (Rhodes et al., 1977). Akella et al. (1976) and Heubner et al. (1976) measured chromium partitioning between olivine and liquid in synthetic systems under conditions compatible with lunar magmatism. Calculations of D_{Cr} for 12008 and 12009 with published data plus those accrued in this study are in agreement with these experimental studies. Akella et al. (1976) found that olivine and liquid did not equilibrate with respect to chromium in cooling rate runs (70°C/hr and 3.5°C/hr). This is consistent with the retention of high Cr-concentrations in the cores of olivine phenocrysts in 12008-12045-12022. It is emphasized that significant reequilibration has occurred in 12016 and 12005. There are no significant titanium variations in olivines among the five analyzed rocks. However, in the coarse-grained samples there is substantial reequilibration between adjacent ilmenite and olivine resulting in higher TiO_2 (up to 0.50 vs. ≈0.10) and lower Mg/(Mg+Fe) in the olivine. One example of this from 12005 is illustrated in Table 3. analyses 7, 8. The details of olivine-spinel equilibration are discussed below in the spinel section.

Discussion of Olivine Chemistry

Rhodes et al. (1977) have modeled near-surface crystal fractionation in the ISBs using 12008 as the parental composition and an olivine of Fo_{72} as the fractionating phase that accounts for most of the compositional variation within the suite. This hypothesis has been tested from a petrographic and phase chemical standpoint in this paper. A related question that is more difficult to evaluate is: Does 12008 represent a primitive, unfractionated magma? One of the criteria which serves to identify basalts that could have crystallized senso stricto

from a liquid is the composition of the most magnesian olivine present in the rock. Using K_D values of 0.33 and 0.30 for Fe-Mg partitioning between liquid and olivine (Roeder and Emslie, 1970), liquidus olivines of Fo_{75} and Fo_{77} are calculated for 12008. The absence of olivine phenocrysts as magnesian as those in 12008 suggests that its present composition is the result of a small net gain of olivine at some point. However, the decreasing cooling rate sequence of 12008→12045→12022 is inferred to represent a stratigraphically descending section at the top of a flow in that decreasing cooling rate correlates positively with degree of olivine subtraction (Rhodes et al., 1977; cf., Walker et al., 1976b). The inverse correlation between the maximum Fo-content of olivine phenocrysts and Mg/(Mg+Fe) of the lava apparently arises from selective loss of early magnesian liquidus olivines from the topmost portion of the flow. One consequence to the compositional variation in phenocrystic olivine produced by monomineralic crystallization with falling temperature is that there will also be a grain size distribution in which phenocryst dimensions and Fo-content correlate positively. The relatively large and magnesian phenocrysts will settle selectively compared to the smaller,lower temperature phenocrysts (Walker et al., 1976b). A second consequence of crystal settling within a lava flow, is that at a given level within the unit (except right at the flow boundaries) there will be partial compensation of phenocrysts from above for those lost downward (e.g., sample 12016 is apparently an example of this process in which a near balance was struck between addition and removal). The most magnesian olivine phenocryst core composition analyzed among the three rocks occurs in 12022, whereas the sample with the lowest maximum Fo-content is 12008. Significantly, the most magnesian olivine phenocryst in 12045 is also larger than any other in the thin section (0.7 mm vs. 0.2-0.5). There are also olivines in 12016 and 12005 that are much larger (1-5 mm) than those in the porphyritic basalts. Although some growth clearly occurred during settling, these large olivines are also embayed, raising

the possibility that they are the remnants of a larger population of such grains now represented by smaller relics. Recognizing that the Fo_{72} olivine composition necessitated by the modeling calculations is probably the average of zoned phenocrysts (e.g., Fo_{76-69}), our findings are compatible with those of Rhodes et al. (1977). Similarily, small amounts of somewhat more iron-rich olivine are required in fractionation modeling of the most evolved ISB samples (i.e., Fo_{69-60}). The range of zoning measured in natural olivine phenocrysts and the presence of Fo_{65} olivine at the olivine-pyroxene-plagioclase cotectic in Green et al's experiments are compatible with this premise.

Spinel

Microprobe analyses of spinels are presented in Table 4 and Figures 7, 8 and 9. The paragenetic sequence of early titanian chromian spinel followed by chromian ulvöspinel recognized in the ISB samples is characteristic of low-titanium mare basalts (Apollo 12 and 15) and has been discussed in detail by El Goresy et al. (1976).

12008: Spinels in 12008 are optically homogeneous, a result confirmed by microprobe analyses that indicate limited chemical zoning entirely restricted to low-titanium compostions. The trend from core to rim is defined by an increase in TiO_2 (6.0→9.9wt.%) accompanied by a slight decrease in Cr/Al (2.5→2.2) and an increase in Fe/(Fe+Mg) from 0.69 to 0.81. Chromian spinel in 12009 is similar in general character to that in 12008 but is 30-50% lower in TiO_2, apparently as a function fo bulk rock chemistry. Donaldson et al. (1976) found that early spinel compositions (12009 experiments) were not a function of cooling rate (70°-7°C/hr) and that at these rapid rates ulvöspinel did not appear.

12045: Early chromian spinels in 12045 partly overlap in composition with those in 12008 and extend the zoning trend of slightly increasing Ti, increasing Fe/(Fe+Mg) and decreasing Cr/(Cr+Al). This composite trend is well displayed in

the Cr:Fe:Mg ternary plot in Figure 7. The combined range of zoning in the two samples is as follows: Ti/(Ti+Cr+Al) = 0.08-0.20, Fe/(Fe+Mg) = 0.68-0.86 and Cr/(Cr+Al) = 0.72-0.70. This composite trend is equivalent to zoning trend #1 of El Goresy et al. (1976). Spinel grains in 12045 that are not protected by enclosure in olivine phenocrysts are zoned to ulvöspinel rims. Skeletal grains of ulvöspinel also occur separately in the groundmass. Optically the boundary between chromian spinel cores and ulvöspinel rims varies from sharp to gradational. The relative degree of idiomorphism of the cores correlates with the sharpness of the break between core and rim compositions. Although these textures are suggestive of minor resorption prior to precipitation of ulvöspinel rims, this paragenesis is not consistent with the rapid cooling history of this sample. The variations in apparent idiomorphism of the chromian spinel cores may be the result of varying geometry between core-rim boundaries and the thin section surface. The rims are compositionally zoned in the same sense as the cores but the relative increase in Ti/(Ti+Cr+Al) is far more abrupt. Ti/(Ti+Cr+Al) increases from 0.2 to 0.6, Fe/(Fe+Mg) increases sharply from 0.87 to 0.91 and thereafter is extended to 0.95, and Cr/(Cr+Al) decreases slightly from 0.70-0.66.

12056: The cooling rate difference between 12045 and 12056 is reflected in a marked change in the spinel parageneses. Relatively small idiomorphic spinel octahedra included within large pyroxene grains exhibit gradational zoning from chromian spinel cores to titanium-rich rims. The zoning trends in these grains are equivalent to these in early 12045 spinels and again are in agreement with trend #1 of El Goresy et al. (1976). Spinel grains not protected by pyroxene are either weakly zoned ulvöspinel with high Fe/(Fe+Mg) = 0.94-0.98 or composite grains of chromian spinel rimmed by ulvöspinel. In the latter case, resorption of earlier chromian spinel occurred prior to the precipitation of later Ti-rich ulvöspinel. In all grains the Cr/(Cr+Al) increases from core to rim. A

characteristic feature of zoning in these spinels is that individual grains zoned from low to high Ti/(Ti+Cr+Al) have variable Fe/(Fe+Mg). Analyses 5, 6, 7 and 8 in Table 4 are examples of core-rim pairs in high-Mg and low-Mg grains. The high Fe/(Fe+Mg) grains are those which are not mantled by pyroxene implying that they are the result of Fe-Mg reequilibration between spinel and the iron-rich residual liquid. Comparison to the 12008-12045 compositions demonstrates that Fe/Mg variations at a given TiO_2-content are not the result of equilibration to lower Fe/(Fe+Mg) between spinel and surrounding pyroxene, as the variation extends to higher, rather than lower, Fe/(Fe+Mg). Busche et al. (1972) recognized similar zoning patterns in ilmenite suite basalt 12051 including a large Fe/(Fe+Mg) spread in chromian spinel. However, we have not analyzed any of the nearly pure end-member ulvöspinel (>30 wt.% TiO_2) which they found.

12016: Spinel parageneses in 12016 are quite similar to those in 12056 with the exception that spinel compositions intermediate between early chromium spinel and Ti-rich ulvöspinel were not analyzed. This may be due to sampling, as relatively few analyses were obtained from this sample. The zoning data available indicate a sharp break between core and rim, a pattern corroborated by petrographic observations which indicate advanced resorption of cores prior to growth of the rim.

12005: Spinel parageneses in 12005 are unique among the samples we have studied in that (1) individual grains exhibit limited zoning and none is a composite of chromian spinel and ulvöspinel and (2) there is an extremely high correlation between spinel composition and the relative order in the crystallization sequence of the enclosing phase (Figure 8a). Spinel enclosed in the cores of early anhedral olivine grains and in the cores of the pyroxene oikocrysts are restricted in composition to chromian spinel with less than 10 wt.% TiO_2. Chromian ulvöspinel is likewise restricted in distribution to the rims of large pyroxenes and the interstitial plagioclase-olivine-pyroxene assemblage. Spinel of a composition

intermediate between the two are predictably located near the core-rim boundaries and in the cores of euhedral olivines within the interstitial assemblage. Linear arrays of spinel grains oriented normal to pyroxene and olivine grain boundaries exhibit compositional changes that mimic the composite trends derived from all the analyses.

Superimposed on these compositional variations are additional effects of subsolidus equilibration. The most pronounced of these is the Fe-Mg exchange between spinel and the enclosing silicates, olivine and pyroxene. Those included in olivine generally have higher Fe/(Fe+Mg) than grains enclosed in pyroxene (Figure 8), indicative of an Fe-Mg exchange in which partitioning of Mg into olivine relative to spinel increases with falling temperature (Irvine, 1965). There is also a substantial difference between Cr/(Cr+Al) in spinels enclosed in olivine vs. pyroxene that implies a decrease in Cr/Al in spinels coexisting with pyroxene. Zoning in the larger grains of chromian spinel included in pyroxene probably records an igneous trend with reequilibration superimposed. The rim to rim microprobe traverse shown in Figure 9 illustrates the combination. The sharp drop in Cr_2O_3 coupled with the slight increase in Al_2O_3 at the rim is inferred to be at least in part the result of reequilibration as the igneous trend is characterized by decreasing Al_2O_3. Note the substantial spread in Cr/Al in the Cr-Ti-Al ternary plot (Figure 8) compared to the other samples. The data of Busche et al. (1972) record similar scatter in Cr/Al for spinels in cumulate 12036. Note also that it is the early spinel which exhibits the largest variation in Cr/Al suggesting that the extent of reequilibration decreased with falling temperature.

One of the spinel grains analyzed in 12005 is an anomalous titanium-poor chromian pleonaste. Three grains with similar compositions were analyzed in 12036 by Busche et al. (1971). The three grains in 12036 have higher Fe/(Fe+Mg) and Al_2O_3 and lower Cr_2O_3 than the 12005 analysis. Taken together, these four analyses

define trends that are not continuous with the other spinels in these rocks in that Cr/Al decreases with increasing Fe/(Fe+Mg) and at the same Fe/(Fe+Mg) they contain far less TiO_2 than the early titanium chromian spinels.

Discussion of Spinel Chemistry

The fundamental differences in the crystallization history and zoning patterns between spinels in slowly cooled and quickly cooled rocks outlined by El Goresy et al. (1976) are present in the ISB spinels. The porphyritic basalts exhibit zoning from early chromian spinel cores to chromian ulvöspinel rims with little or no resorption of the first phase prior to precipitation of the rims. Resorption textures are well developed in the medium-grained basalts resulting in composite trends. Haggerty and Meyer (1970) found a compositional gap in spinels from the partial olivine cumulates 12020 and 12040 and the medium-grained, equigranular pigeonite suite basalt 12064 (similar to that observed in 12016). Busche et al. (1972) recognized the same bimodal distribution in the highly evolved feldspathic microgabbro 12038. The absence of the gap in more slowly cooled rocks such as 12005 and 12036 as well as more quickly cooled samples 12051, 12056 and 12045 suggests that the combination of resorption of early chromian spinel followed by plating-on of chromian ulvöspinel is favored by intermediate cooling rates.

A third distinct pattern of textural-chemical variation is present in 12005 spinels. Idiomorphic chromian spinel in the cores of pyroxene oikocrysts that does not show Ti-enrichment beyond the range present in 12008 is inferred to have accumulated (along with olivine phenocrysts) during the initial phase of crystal settling. The absence of ulvöspinel rims is probably due to the buffering effect of the olivine-liquid peritectic reaction that led to the growth of the large pyroxene oikocrysts which enveloped the low-Ti spinels. The presence of the first

substantially Ti-enriched spinel at the core-rim boundary of the pyroxene oikocrysts suggests that it formed in response to a change in residual liquid composition although falling temperature may also be a factor in controlling spinel compositions. The Ti-Al substitution relations in the pyroxenes indicate that the core-rim boundary coincides with the incoming of plagioclse (see below). One possible interpretation is that the spinels with TiO_2 >10 wt. percent are free-grown grains that formed with something like their present composition in response to the gradually changing liquid composition. A second is that spinel more enriched in the ulvöspinel component than the initial composition is the result of complete reaction (combination of resorption and reequilibration) between early spinel and the evolving liquid composition. The second mechanism is considered most likely because the early cumulate spinels were probably distributed throughout the rock and not segregated in the areas which became the cores of pyroxene oikocrysts. In either case, the limited range of zoning in these spinels and the correspondence between composition and crystallization sequence are consistent with very slow cooling through the temperature range in which spinel formed. Note also that the maximum Ti-content of ulvöspinel in 12005 is less than in 12045, 12016 or 12056, consistent with its less evolved residual liquid and the extensive subsolidus reduction (El Goresy and Ramdohr, 1975).

One unlikely possibility for the origin of the pleonaste spinel is that it represents the true low-pressure liquidus phase or a high pressure phase which, with falling temperature, tends to react out. None of the experimental studies of low-titanium mare basalts record such spinels but the ratio of spinel to melt would be limited by the initial Cr-contents of the magmas suggesting that they could be overlooked in the rocks and in experimental charges. A more probable alternative is that they are refractory xenocrystal material plucked from anorthositic or KREEPy basement rocks or their regolith prior to eruption. Although these anomalous spinels are the only petrographic evidence for assimilation in the Apollo 12 basalts,

the aberrant trace element characteristics (Rhodes et al., 1977) and $^{87}Sr/^{86}Sr$ initial ratio (Nyquist et al., 1977) of sample 12036 provide some support for the presence of a very small amount of exotic material.

Pyroxene: Porphyritic Basalts

Augite phenocrysts in the porphyritic ISBs vary in morphology from dendrites (12008) to highly elongate (12045) to less elongate (12022) within the cooling rate sequence in which there is also an increase in the grain size and relative proportions of the phenocrysts. There are also marked variations in pyroxene composition among these nearly isochemical basalts (Table 5; Figures 10, 11, 12). Dendrites in 12008 and phenocrysts in 12045 and 12022 all plot near the diopside-hedenbergite join as do pyroxenes from quickly cooled Apollo 11 and 17 high-Ti basalts. They also have similarly high Ti- and Al-contents (e.g., Brown et al., 1975) and Ti:Al = 0.35 - 0.52. Dendrites in 12008 have higher Cr_2O_3 than the other samples (Figure 12). The vertical trend on the quadrilateral (Figure 10a) is apparently the result of Ca-enrichment with progressive crystallization as the low-calcium compositions are highest in Cr. Zoning trends in these extremely fine-grained dendrites have not been documented in detail but similar trends were found by Donaldson et al. (1975) in cooling rate runs on a 12009 analog composition. In 12045 and 12022 there are two distinct generations of pyroxene, phenocrysts and groundmass, which have markedly different compositions. The pyroxene overgrowths on olivine phenocrysts and discreet pyroxene phenocrysts in 12045 are equivalent in composition and exhibit decreasing in Ti, Cr, Al and Ca with iron-enrichment in core to rim zoning. The compositional hiatus between phenocrysts and groundmass pyroxene is most dramatically expressed in lower Ti, Al and Cr concentrations (Figures 11 and 12). Individual grains are also strongly zoned with respect to Fe/Mg from core to rim with the latter approaching

compositions near the ferrosilite-hedenbergite join (Figure 10a). The groundmass pyroxenes in 12045 and 12022 are essentially identical in composition, apparently as the result of rapid co-crystallization with plagioclase and ilmenite at substantial undercooling.

Pyroxene: Medium and Coarse Grained Basalts

Microprobe analyses of pyroxene in 12056, 12016 and 12005 were collected primarily along linear traverses from core to rim or from rim to rim (10-25 points). Beginning and end points were pre-selected with the locations of intervening analysis points determined automatically by equal-increment spacing along the traverse. Although small grains intergrown with plagioclase were analyzed, the majority of analyses were made on large grians. The traverses were oriented normal to optical zoning boundaries that are generally parallel to the long dimension of the grains. This mode of data collection results in an unbiased survey reflecting the entire range of pyroxene compositions in the sample. However, where zoning trends are complex (e.g., intergrowths of high-calcium and low-calcium pyroxene) fine details may remain unresolved. In this study the distance between points (20 μm - 100 μm) was, in some cases, greater than the scale of two-pyroxene intergrowths which are present in these rocks.

Pyroxene analyses of 12056, 12016 and 12005 have been divided into cores and rims in plotting them on Figures 10, 11 and 12. These distinctions have been made on the basis of location within the individual grain with respect to discrete zoning boundaries and certain compositional parameters (Fe/Fe+Mg, Cr_2O_3 and Ti:Al) which tend to vary discontinuously across these zoning boundaries. However, in some traverses the compositional variations were continuous or different parameters were conflicting. Thus, the graphical distinction may be arbitrary for some points in the compositional ranges close to the core-rim boundaries. The internal zoning patterns of individual pyroxenes in the three rocks exhibit significant variation among the three rocks and are discussed separately below.

12056: The cores of large grains are dominated by augite although small amounts of low-calcium pyroxene are present. Hollister et al. (1971) found a similar pattern in the cores of 12063 pyroxenes, a rock close to 12056 in bulk composition and cooling history. They performed zoning traverses with very closely spaced points acorss a few grains and found that the low-calcium phase apparently respresents the innermost core, implying that the augite followed the low-calcium pyroxene in the crystallization sequence and nucleated epitaxially on it. If this inference is correct, it may reflect initial precipitation of a low-calcium pyroxene as the result of the olivine-liquid peritectic. Both 12063 and 12056 exhibit a discontinuity on the pyroxene quadrilateral between cores and rims. Individual zoning trends in rims are illustrated by arrows on the quadrilateral plot (Figure 10). Titanium and aluminum zoning in cores and rims is oscillatory and is generally positively correlated with Ca-content.

12016: Pyroxene zoning trends in 12016 are the most complex of the medium- to coarse-grained rocks, primarily due to abundant intergrowths of high-calcium and low-calcium pyroxene in both cores and rims. Arrows tracing the individual zoning trends are not shown on the quadrilateral plot in order to avoid clutter as they tend to be quite irregular. Like 12056, most symmetrically zoned grains in 12016 have augite cores intergrown with minor low-calcium pyroxene or subcalcic augite. These relationships have not been entirely resolved in genetic terms. A compositional hiatus between core and rim is not evident in the composite plot of analyses on the quadrilateral but it does occur in some of the individual grains.

12005: The majority of large grains are composed of augite cores rimmed by low-calcium pyroxene. Rim augite is most typically present in the outermost margin intergrown with the low-calcium phase. However, several of the largest grains include augite plus low-calcium pyroxene intergrowths in their cores.

Locally, resorbed olivine grains are partly mantled by low-calcium pyroxene, again suggesting the two-pyroxene intergrowths are the result of a peritectic reaction. The lack of any truly subcalcic compositions contrasts with all the other samples studied (including 12036-Busche et al., 1971) and may indicate an approach to an equilibrium solvus. The complete separation of augite and low-calcium pyroxene on the quadrilateral is matched by non-overlap between the two phases on the Ti-Al and Cr_2O_3 vs. Fe/(Fe+Mg) plots.

Discussion of Pyroxene Chemistry

Compositional differences between pyroxenes in the porphyritic basalts and the medium- to coarse-grained basalts are ascribed to the distinctly different cooling histories inferred for the two groups. The presence of only augite with high Ti and Al as well as high Ti:Al in 12008, 12045, 12022 and the rapidly cooled Apollo 11 and 17 high-titanium basalts is a characteristic expression of the relatively high titanium contents of the rocks and the crystallization of pyroxene at substantial undercooling. The cooling rate dependence of augite phenocrysts in the porphyritic ISBs is demonstrated by its absence (pyroxene phase = pigeonite) in isothermal melting experiments on 12022 (Green et al., 1971). Higher bulk titanium appears to favor augite over low-calcium pyroxene in rapidly cooled rocks as the latter phase is the dominant pyroxene in porphyritic olivine suite basalts such as 12002 (Walker et al., 1976a) which appears to have had a cooling rate history similar to 12022.

Within the three porphyritic basalts there are also major differences among the three rocks that are inferred to be controlled by cooling rate. Although the augite phenocrysts in 12022 and 12045 plot in similar positions in terms of quadrilateral components they have quite different characteristics in terms of their Ti-Al relations. In contrast to the Ti and Al decrease with progressive crystallization in 12045 phenocrysts, those in 12022

(Weill et al., 1971; Bence and Papike, 1972) show an increase in Ti and Al from core to rim and have lower Ti:Al ratios (0.33) as opposed to 12045 (0.35 - 0.52). The much lower Ti and Al in the cores of the 12022 phenocrysts is due to less supression of the temperature of appearance of pyroxene compared to 12045, whereas the increase in these components from cores to rims (in 12022) apparently reflects crystallization at increasing undercooling (Kirkpatrick, 1976). The 12045 phenocrysts also crystallized with progressively greater undercooling, but the initial titanium-content in these pyroxenes is substantially greater than in the bulk composition suggesting that Ti-depletion of the residual liquid may be responsible for the trend.

In contrast to the porphyritic basalts, low-calcium pyroxene comprises a significant proportion of the pyroxene in the three medium- to coarse-grained rocks. The ratio of low-calcium pyroxene to augite increases in the sequence 12056→12016→12005 (Table 2). Within the same sequence there is a progressive change in the Ti:Al relations that appears to correspond to cooling rate differences (Figure 11b, c, d). The maximum titanium and aluminum concentrations in the 12056 augites exceed those in 12016 and 12005. In all three rocks the low-calcium and high-calcium compositions in the cores of large grains have the same Ti:Al with the low-calcium pyrexene containing lower concentrations of Ti and Al as well as Cr (Figures 11, 12).

In all three rocks there are optical zoning boundaries between core and rim across which there is a marked shift to lower Ti, Al and Cr accompanied by an increase in Ti:Al to ≈1:2 and a decrease of octahedral Al to zero. The ratio of 1:2 is typical of lunar pyroxenes crystallizing with plagioclase and the decrease in Ti and Al concentrations apparently marks the effect of ilmenite and plagioclase co-precipitation, depleting the residuum in these components.

However, for a given rock the composite of many analyses indicates that there tends to be a gradation between core and rim compositions with respect to these elements. This pattern of gradual Ti-Al decrease contrasts with the phenocryst-groundmass relations in the porphyritic basalts. This is apparently due to the very rapid growth of plagioclase and ilmenite at substantial undercooling in more quickly cooled rocks as compared to the more slowly cooled samples in which there is a closer approach to equilibrium crystallization.

The degree of iron-enrichment in the ISB pyroxenes also varies substantially due to the cooling rate dependence of residual liquid fractionation. As expected, the most fractionated liquids are found in the porphyritic basalts in which the strongly zoned groundmass pyroxenes approach the hedenbergite-ferrosilite join. The Mg/(Mg+Fe) ranges of the pyroxenes in the three medium- and coarse-grained basalts are 12056 - 0.70 to 0.15, 12016 - 0.71 to 0.27 and 12005 - 0.75 to 0.63. The marked contrast between the 12005 pyroxenes and those in 12056 - 12016 is the result of the extensive adcumulus growth in the former.

Feldspar

A survey of the range of plagioclase compositions in 12056, 12016 and 12005 (Table 6; Figure 13) was obtained by analyzing cores and rims of several grains in each sample. The plagioclase composition at various stages of crystallization has been monitored by analyzing grains of various sizes and morphologies ranging from large and equant (early) to small lath-shaped grains (late). The Fe-Mg zoning in mare basalt plagioclase parallels the increase in Fe/Mg in coexisting liquid during progressive crystallization and can, therefore, be used as an index of fractionation against which An-Ab-Or variations in the plagioclase can be compared (e.g., Longhi et al., 1976).

The cores of large equant grains are the most calcic compositions analyzed in all three rocks and also have the lowest Fe/(Fe+Mg). The cores of smaller lath-shaped plagioclase, that apparently formed later in the crystallization sequence (in any given rock) than the large blocky grains, have intermediate Fe/(Fe+Mg) which varies with proximity to mesostasis segregations. Within the fractionation-cooling rate sequence 12056→12016→12005 the most calcic plagioclases analyzed have successively lower Fe/(Fe+Mg) and higher An-contents (12056 = 0.55 - 88; 12016 = 0.51 - 91; 12005 = 0.43 - 93). This progression is consistent with predictions of the effect of plagioclase nucleation at decreasing increments of undercooling. The trend to higher An-content of the initial plagioclase may signify progressively less depression of the plagioclase liquidus from 12056→12016→12005 with decreasing cooling rate. This is corroborated by an increase in An-content in the 12056 plagioclases at Fe/(Fe+Mg) of 0.65 - 0.75. Lofgren (1973) showed that suppression of plagioclase crystallization at large undercoolings can result in reverse zoning of this type. Similar zoning relationships have been recognized in 12021 (Crawford, 1973) and 12002 (Longhi et al., 1976).

The late stage enrichment of iron over magnesium in plagioclase follows the pattern observed for olivine and pyroxene: the enrichment approaches an Fe/(Fe+Mg) = 1.0 in both 12016 and 12056 and is less extreme in 12005 (0.78). The late stage enrichment in potassium at a given Fe/(Fe+Mg) varies substantially among the three rocks.

Rim compositions in 12005 adjacent to and intergrown with K-feldspar and phosphate (i.e., holocrystalline mesostasis segregation) are sodic bytownite ($An_{78-73}\ Ab_{16-21}\ Or_{5-7}$). These are among the most sodic plagioclases analyzed in mare basalts (cf., Papike et al., 1976). The most sodic plagioclase in 12036 is also bytownite with a high potassium-content (Or_5) indicating a similar zoning pattern (Keil et al., 1971). Aided by a slow crystallization rate and

abundant trapped liquid, plagioclase zoning in 12005 was suppressed, both in terms of An-Ab-Or and Fe/(Fe+Mg). Plagioclase rims, which grew adjacent to rare segregations of mesostasis, record the strong alkali-enrichment in a vanishingly small amount of residual liquid.

The late stage enrichment of alkalis in 12056 and 12016 can be directly contrasted due to similar degrees of iron-enrichment and the presence of discrete alkali-rich phases in their mesostasis segregations. Relative to 12016, the Na + K-enrichment in 12056 plagioclases at Fe/(Fe+Mg) >0.70 is suppressed (Figure 13b). The symplectoid intergrowths in mesostasis segregations of 12056 are considered evidence of immiscibility in the residual liquid of 12056 at a less advanced stage of crystallization than in 12016, which lacks these intergrowths. It is suggested that plagioclase crystallization from the iron-rich, alkali-depleted immiscible fraction produces plagioclase with similar characteristics. Powell et al. (1976) proposed this mechanism as an explanation for the high An-contents of acicular plagioclase in the mesostasis of highlands melt rocks analogous to those described by Brown and Peckett (1972). As the ratio of the iron-rich to silica- and potassium-rich immiscible fractions is generally high, plagioclase adjacent to mesostasis segregations would most likely be in contact with the iron-rich phase rather than the silica-rich fraction which is dispersed as small blebs. Non-equilibrium crystallization from the iron-rich liquid could account for the observed alkali-enrichment trends in the 12056 and 12016 plagioclases.

Potassium feldspar occurs in the holocrystalline mesostasis of 12005 (Analysis 9, Table 6) and 12016. The silica and potassium-rich phase in the mesostasis segregations of 12016 and 12056 appears to be primarily composed of a glass although Trzcienski and Kulick (1972) identified a barium-rich K-feldspar in the mesostasis of 12063. The composition of the alkali-rich glass in 12016 is as follows: SiO_2 = 61.98, TiO_2 = 0.21, Al_2O_3 = 22.0, FeO = 1.07, MgO = 0.02,

CaO = 1.00, Na_2O = 0.32, K_2O = 11.61, BaO = 0.12. A barium phase was sought in the mesostasis areas but was not located. Barium-contents in most analyzed plagioclase grains were below detection limits but some rims adjacent to mesostasis contained resolvable amounts (0.01 - 0.10 wt.% BaO).

Ilmenite

A wide variety of ilmenite morphologies is present in the ISBs. The change from skeletal plates to more equant forms correlates with cooling rate (Usselman et al., 1975). The wispy filamental ilmenite (<1 μm) in 12008 is too fine-grained to be analyzed with the microprobe but the thin skeletal plates in 12045 (1-10 μm) and 12022 (5-25 μm) and the more coarse-grained laths and blocky grains in the other samples in the suite have been analyzed in this study (Figure 14) or by other workers.

Ilmenite in 12045 is nearly stoichiometric $FeTiO_3$ with MgO <0.1 in most grains (one at 0.4 wt.% MgO) and Cr_2O_3 <0.2 wt.%. Similar compositions with slightly higher MgO (0.4 - 0.6 wt.%) were found for ilmenite in 12022 (Weill et al., 1971; Cameron, 1971). The MgO-contents of ilmenite in the medium-grained basalts are more variable and higher. Grain to grain variations in ilmenite composition in 12016 and 12056 are much greater than within individual grains. Ilmenite within or adjacent to mesostasis segregations is low in MgO and Cr_2O_3 relative to those intergrown with plagioclase and ferromagnesian minerals. Ilmenite with a similar compositional range (0.11 - 1.68 wt.% MgO) is present in the evolved, medium-grained ISB 12051 (Keil et al., 1971). Ilmenite in 12005 is characterized by a narrow compositional range and high MgO and Cr_2O_3 relative to 12016 and 12056. Keil et al. (1971) report MgO-contents of 3.0 - 4.6 wt.% in 12036, consistent with its intermediate chemistry and lack of iron enrichment in its late-stage mesostasis relative to 12016 and 12056. Similar patterns of ilmenite compositional variation are present in fine-grained and coarse-grained

members of the Apollo 12 olivine suite (e.g., El Goresy et al., 1971). These observations are consistent with the conclusion of Usselman (1975) that ilmenite compositions are controlled by reequilibration with residual liquid and coexisting ferromagnesian phases.

Metal

Metallic iron appears to have been a stable phase throughout most, if not all, of the crystallization history of the ISBs. It occurs in the rims of olivine phenocrysts in porphyritic basalts and is commonly intergrown with early spinel in all the samples studied. Metal inclusions have not been observed in the cores of olivine phenocrysts, except as the crystallization products of melt inclusions. Hewins and Goldstein (1974) recognized the same pattern in a detailed study of metal-olivine relationships in 12004 and 12022. Consequently, it has not been demonstrated that the parental liquid of the ISBs was saturated with metallic iron under the P-T-f_{O_2} conditions at which liquidus olivine precipitated. The textural relations are compatible with the presence of a metal phase on eruption and do not preclude earlier metal saturation since the small number and grain size of the metal grains may account for the negative observation. However, modeling of Ni-Co fractionation in 12022 by Hewins and Goldstein (1974) suggests that olivine crystallized alone prior to the onset of metal saturation.

Brett et al. (1971) and Reid et al. (1970) analyzed metal in several Apollo 12 basalts including 12008 and 12022. Early metal enclosed in olivine phenocrysts tends to be strongly enriched in Ni (30-56% Ni) relative to the slightly later and more abundant population intergrown with spinel. Metallic iron abundances reported in Gibson et al. (1977) indicate an accumulation of this phase in 12016, 12036 and 12005 relative to all the other ISB samples,consistent with the presence of metal inclusions in cumulus olivine and spinel. 12008 contains much less metal than 12045 (220 vs. 520 ppm) apparently as the result of quenching, which acted to suppress the

growth of groundmass metal. In the medium- to coarse-grained basalts metal tends to be concentrated in the mesostasis segregations where it is typically intergrown with troilite. It also occurs associated with reduction assemblages in ilmenite and ulvöspinel where it forms veins crosscutting silicates and oxide phases and as micron-sized disseminated blebs. As noted above, the intensity of subsolidus reduction increases from 12056→12016→12005.

Three element analyses (Ni-Co-Fe) of metal in 12056, 12016 and 12005 are reported in Figure 15. Metal grains intergrown with late-stage phases, such as troilite, in 12056 and 12016 are characterized by very low Ni and Co consistent with concentration of these elements in early crystallizing metal. Metal within olivine in 12056 has the highest Ni of any analyzed. Keil et al. (1971) report Ni-Co relations in metal of 12051 very similar to those in 12016 and 12056. Metal in 12005 (this study) and 12036 (Keil et al., 1971) is characterized by relatively constant Co (1-2.5 wt.%) and Ni-contents which are intermediate between the strongly Ni-enriched early metal in olivine phenocrysts (>20 Ni wt.%) and the low-Ni late-stage metal associated with mesostasis segregations (<3-6 Ni wt.%). A similar pattern of Ni-Co variation was found by Dowty et al. (1974) in a range of textural types in Apollo 15 mare basalts (see their Figure 8). The higher average Ni-content of the metal grains in the cumulates (12036-12005) probably reflects the presence of partly equilibrated Ni-rich metal added during olivine accumulation. This compositional pattern is similar to that recorded in ISB ilmenites.

VI. Summary and Conclusions

As vertical cross sections of lunar lava flows have been sampled by random impact excavation rather than systematic collection from continuous outcrop, reconstruction of petrogenetic relationships among cogenetic rocks must proceed by the interpretation of data gathered from the individual samples. Our ability

to make such a reconstruction hinges on the assumptions that (1) the degree of differentiation indicated by the bulk chemistry of individual samples is a function of the cooling history at that particular location in the flow and (2) that each sample will have recorded in its mineralogy and textures a unique crystallization history. An internally consistent conceptual framework within which all the ilmenite suite basalts can be related has emerged in the integration of combined mineral chemistry data and petrographic interpretations with a fractionation model determined independently on the basis of bulk chemistry (Rhodes et al., 1977). The major conclusion we have derived from this petrologic synthesis is that the bulk chemical variations in the ilmenite suite can be reconciled with differentiation within a single cooling unit. The critical observation is that included within the suite there are (1) olivine-porphyritic basalts, (2) medium-grained basalts with evolved compositions that can be related to the porphyritic basalts by subtraction of olivine and (3) their complementary derivatives, partial olivine cumulates.

The three olivine porphyritic basalts 12008 (vitrophyre), 12045 and 12022 (variolitic groundmasses) comprise a decreasing cooling rate sequence corresponding to increasing olivine removal (up to seven percent in 12022). The progressive coarsening of the groundmass phases and variations in the morphologies of various minerals that are produced by crystallization at different degrees of undercooling are clear indications of the cooling rate sequence. The Ti-Al relations among the phenocrystic and groundmass pyroxenes very in a way entirely consistent with this sequence. On the basis of these relationships, the porphyritic basalts are inferred to represent the chilled carapace of the flow and the cooling rate hierarchy (fast→slow) is presumed to reflect a descending stratigraphic sequence. Walker et al. (1976b) reached an analogous conclusion for the Apollo 12 olivine basalt suite using a somewhat different approach. On the basis of a monotonic covariance between decreasing cooling rate and increasing olivine accumulation, they inferred that the olivine basalts (varying from vitrophyres to partial cumulates) represent samples from the base of a single flow.

The medium-grained, ophitic to subophitic, evolved basalts (12047, 12054, 12051, 12063 and 12056) are the best represented textural-chemical type among the ilmenite suite basalts. These are quite distinct texturally from the porphyritic basalts and have had much slower cooling histories. Chemically these range from quartz-normative basalts from which olivine-removal has been 100 percent efficient (12047, 12054 and 12051) to less fractionated variants that have retained some of the original phenocrystic olivine (12063 and 12056). The inferred descending stratigraphic sequence corresponds to decreasing cooling rate and decreasing olivine removal. These trends exhibit the inverse correlation found among the porphyritic basalts. As a group they must have formed in the upper portion of the flow, below the porphyritic basalts and above the cumulates.

Sample 12016 is also an equigranular, medium-grained basalt. Its major element bulk chemistry is very much like the porphyritic basalts but its textures are indicative of a cooling history intermediate between the evolved basalts and the more slowly cooled cumulates. Consequently, its stratigraphic position also must have been intermediate between the zones of olivine removal and accumulation so that the amount lost by settling was just compensated for from above.

Mineral chemistry variations measured in 12056 and 12016 that are dependent on cooling rate (e.g., pyroxene compositions, spinel parageneses and mineral reequilibration) are entirely consistent with radically lower cooling rates for the medium-grained basalts compared to the porphyritic basalts and with the detailed stratigraphic inferences. Most of the chemical variation among the ISBs can be accounted for by fractional crystallization of olivine with the composition of Fo_{72} plus minor chromian spinel and metal. This is consistent with the compositions of olivine phenocrysts in the porphyritic basalts. However, in the most evolved ISBs additional small amounts of more iron-rich olivine (Fo_{69-60})

are required in the modeling calculations (Rhodes et al., 1977). All the medium-grained basalts contain strongly zoned pyroxene and minor fayalite + silica + alkali-rich glass in their residual mesostases indicating substantial internal fractionation.

The fractionation modeling calculations of Rhodes et al. (1977) require approximately 30 percent olivine accumulation from a parent of 12008 composition to produce 12005. This sample is consequently the most extreme example of a mare basalt cumulate thus far recognized in the Apollo collection. Sample 12036 is tentatively included in the ISBs despite some anomalous chemical characteristics (Rhodes et al., 1977). In virtually all respects (mineral chemistry, modal mineralogy and bulk chemistry) it is intermediate between 12016 and 12005. However, pyroxene must also be involved as a fractionating phase in the cumulates. Petrographic support for this comes from the presence of large pyroxene oikocrysts in 12005 (and 12036) that include abundant embayed and rounded olivine. These features are interpreted as evidence for extensive adcumulus growth of pyroxene and an olivine-liquid peritectic reaction. Thus, the pyroxene is not a cumulus phase but a product of diffusion in intercumulus liquid. A second allied deviation from simple olivine fractionation is necessitated by the fact that the medium-grained evolved basalts and cumulates are enriched and depleted respectively in magmaphile elements (e.g., Fe, Ti, K, P and REE) relative to calculated values derived from modeling the fractionation on major elements and trace elements that are preferentially incorporated into early crystallizing phases (e.g., Co, Ni and Cr). Sample 12016 is particularly enriched in magmaphile elements as befits its inferred stratigraphic position immediately above the cumulate horizon. This complexity is entirely consistent with the paucity of residual mesostasis and the unusually limited iron-enrichment recorded in the ferromagnesian minerals of 12005 and 12036.

Additional features that are indicative of slow cooling in the presence of abundant intercumulus liquid abound in 12005. The plagioclase exhibits restricted Fe/Mg but greater than normal alkali-enrichment. Spinel parageneses are unique in that none of the individual grains is zoned from titanian chromium spinel to chromium ulvöspinel even though the composite of spinel analyses shows an unbroken range between the most titanium-poor and titanium-rich compositions. The pyroxenes record evidence for slow cooling in their relatively coarse exsolution lamellae, low Ti and Al and low Ti:Al plus an absence of compositions with calcium-contents intermediate between augite and low-calcium pyroxene. The latter may be indicative of an approach to an equilibrium solvus.

Acknowledgements

We are indebted to Bob Myers and Ken Edloe (LEC) for software development in conjunction with automation of the MAC microprobe. Gary Lofgren and J. M. Rhodes contributed numerous invaluable insights concerning mare basalt petrology and geochemistry. An exceptionally thourough review by S. A. Morse contributed to improvement of the original manuscript. Elinor Stockton, Linda Dungan and Lina Romero assisted in preparation of the manuscript.

Akella J., Williams R. J. and Mullins O. (1976) Solubility of Cr, Ti, and Al in co-existing olivine, spinel, and liquid at 1 atm. Proc. Lunar Sci. Conf. 7th, p. 1179-1194.

Brett R., Butler P., Meyer C., Reid A. M., Takeda H. and Williams R. (1971) Apollo 12 igneous rocks 12004, 12008, 12009, and 12022: A mineralogical and petrological study. Proc. Lunar Sci. Conf. 2nd, p. 301-317.

Brown G. M. and Peckett A. (1971) Selective volatilization on the lunar surface: Evidence from Apollo 14 feldspar phyric basalts. Nature 234, p. 262-266.

Brown G. M., Emeleus C. H., Holland J. G., Peckett and Phillips R. (1971) Picrite basalts, ferrobasalts, feldspathic norites, and rhyolites in a strongly fractionated lunar crust. Proc. Lunar Sci. Conf. 2nd, p. 583-600.

Brown G. M., Peckett A., Emeleus C. H., Phillips R. and Pinsent R. H. (1975) Petrology and mineralogy of Apollo 17 mare basalts. Proc. Lunar Sci. Conf. 6th, p. 1-13.

Busche F. D., Conrad G. H., Keil K., Prinz M., Bunch T. E., Erlichman J. E. and Quaide W. L. (1971) Electron microprobe analyses of minerals from Apollo 12 lunar samples. Univ. New Mexico, Inst. Meteoritics, Spec. Pub. 3, 61p.

Busche F. D., Prinz M., Keil K. and Bunch T. E. (1972) Spinel and the petrogenesis of some Apollo 12 igneous rocks. Amer. Min. 57, p. 1729-1747.

Butler P., Jr. (1972) Compositional characteristics of olivines from Apollo 12 samples. Geochim. Cosmochim. Acta, 36, p. 773-785.

Cameron E. N. (1971) Opaque minerals in certain lunar rocks from Apollo 12. Proc. Lunar Sci. Conf. 2nd, p. 193-206.

Compston W., Berry H., Vernon M. J., Chappell B. W. and Kaye M. J. (1971) Rb-Sr chronology and chemistry of lunar material from the Ocean of Storms. Proc. Lunar Sci. Conf. 2nd, p. 1471-1485.

Crawford M. L. (1973) Crystallization of plagioclase in mare basalts. Proc. Lunar Sci. Conf. 4th, p. 705-717.

Donaldson C. H., Usselman T. M., Williams R. J. and Lofgren G. E. (1975) Experimental modeling of the cooling history of Apollo 12 olivine basalts. Proc. Lunar Sci. Conf. 6th, p. 843-869.

Donaldson C. H., (1976) An experimental investigation of olivine morphology. Contrib. Mineral. Petrol. 57, p. 187-213.

Dowty E., Prinz M. and Keil K. (1973) Composition, mineralogy and petrology of 28 mare basalts from Apollo 15 rake samples. Proc. Lunar Sci. Conf. 4th, p. 423-444.

El Goresy A., Ramdohr P. and Taylor L. A. (1971) The opaque minerals in the lunar rocks from Oceanus Procellarum. Proc. Lunar Sci. Conf. 2nd, p. 219-235.

El Goresy A. and Ramdohr P. (1975) Subsolidus reduction of lunar opaque oxides: Textures, assemblages, geochemistry, and evidence for a late stage endogenic gaseous mixture. Proc. Lunar Sci. Conf. 6th, p. 729-745.

El Goresy A., Prinz M. and Ramdohr P. (1976) Zoning in spinels as an indicator of the crystallization histories of mare basalts. Proc. Lunar Sci. Conf. 7th, p. 1261-1279.

Engel A. E. J., Engel C. G., Sutton A. L. and Myers A. T. (1971) Composition of five Apollo 11 and Apollo 12 rocks and one Apollo 11 soil and some petrogenetic considerations. Proc. Lunar Sci. Conf. 2nd, p. 439-448.

Gibson E. K., Jr. (1977) Sulfur in lunar mare basalts as a function of bulk composition. Proc. Lunar Sci. Conf. 8th, in press.

Green D. H., Ringwood A. E., Ware N. G., Hibberson W. O., Major A. and Kiss E. (1971) Experimental petrology and petrogenesis of Apollo 12 basalts. Proc. Lunar Sci. Conf. 2nd, p. 601-615.

Haggerty S. E. and Meyer H. O. A. (1970) Apollo 12: Opaque oxides. Earth Planet. Sci. Lett. 9, p. 379-387.

Hewins R. H. and Goldstein J. I. (1974) Metal-olivine associations and Ni-Co contents in two Apollo 12 mare basalts. Earth Planet. Sci. Lett. 24, p. 59-70.

Hollister L. S., Trzcienski W. E., Jr., Hargraves R. B. and Kulick C. G. (1971) Petrogenetic significance of pyroxenes in two Apollo 12 samples. Proc. Lunar Sci. Conf. 2nd, p. 529-557.

Huebner J. S., Lipin B. R. and Wiggins L. B. (1976) Partitioning of chromium between silicate crystals and melts. Proc. Lunar Sci. Conf. 7th, p. 1195-1220.

Irvine T. N. (1965) Chromian spinel as a petrogenetic indicator. Part I, Theory. Can. J. Earth Sci. 2, p. 648-672.

James O. B. and Wright T. L. (1972) Apollo 11 and 12 mare basalts and gabbros: Classification, compositional variations, and possible petrogenetic relations. Bull. Geol. Soc. Amer. 83, p. 2357-2382.

Keil K., Prinz M. and Bunch T. E. (1971) Mineralogy, petrology, and chemistry of some Apollo 12 samples. Proc. Lunar Sci. Conf. 2nd, p. 319-341.

Kirkpatrick R. J. (1976) Towards a kinetic model for the crystallization of magma bodies. J. Geophys. Res. 81, p. 2565-2571.

Kushiro I. and Haramura H. (1971) Major element variation and possible source materials of Apollo 12 crystalline rocks. Science 171, p. 1235-1237.

Lofgren G. E. (1973) Temperature induced zoning in synthetic plagioclase feldspar. In The Feldspars, p. 362-375. Manchester Univ. Press.

Lofgren G. E. and Gooley R. (1977) Simultaneous crystallization of feldspar intergrowths from the melt. Am. Min. 62, p. 217-228.

Longhi J., Walker D. and Hays J. F. (1976) Fe and Mg in plagioclase. Proc. Lunar Sci. Conf. 7th, p. 1281-1300.

Moore J. G. and Evans B. W. (1967) The role of olivine in the crystallization of the prehistoric Makaopuhi tholeiitic lava lake. Contrib. Mineral. Petrol. 15, p. 202-223.

Papike J. J., Hodges F. N., Bence A. E., Cameron M. and Rhodes J. M. (1976) Mare Basalts: Crystal chemistry, mineralogy, and petrology. Rev. Geophys. Space Phys. 14, p. 475-540.

Powell B. N., Dungan M. A. and Weiblen P. W. (1975) Apollo 16 feldspathic melt rocks: Clues to the magmatic history of the lunar crust. Proc. Lunar Sci. Conf. 6th, p. 415-433.

Nyquist L. E., Bansal B. M., Wooden J. L. and Wiesmann H. (1977) Sr-isotopic constraints on the petrogenesis of Apollo 12 mare basalts. Proc. Lunar Sci. Conf. 8th, in press.

Reid A. M., Meyer C., Jr., Harmon R. S. and Brett R. (1970) Metal grains in Apollo 12 igneous rocks. Earth Planet. Sci. Lett. 9, p. 1-5.

Rhodes J. M., Blanchard D. P., Brannon J. C., Rodgers K. V. and Dungan M. A. (1977) Chemistry, classification and petrogenesis of Apollo 12 mare basalts. Proc. Lunar Sci. Conf. 8th, in press.

Roeder P. L. and Emslie R. F. (1970) Olivine-liquid equilibrium. Contrib. Mineral. Petrol. 29, p. 275-289.

Schaal R. B. and Hörz F. (1977) Shock metamorphism of lunar and terrestrial basalts. Proc. Lunar Sci. Conf. 8th, in press.

Trzcienski W. E., Jr. and Kulick C. G. (1972) Plagioclase and Ba-K phases from Apollo samples 12063 and 14310. Proc. Lunar Sci. Conf. 3rd, p. 591-602.

Usselman T. M. (1975) Ilmenite chemistry in mare basalts, an experimental study. In Origins of Mare Basalts and their Implications for Lunar Evolution, p. 164-168.

Usselman T. M., Lofgren G. E., Donaldson C. H. and Williams R. J. (1975) Experimentally reproduced textures and mineral chemistries of high-titanium mare basalts. Proc. Lunar Sci. Conf. 6th, p. 997-1020.

Walker D., Kirkpatrick R. J., Longhi J. and Hays J. F. (1976a) Crystallization history of lunar picvitic basalt sample 12002: Phase equilibria and cooling rate studies. Bull. Geol. Soc. Am. 87, p. 646-656.

Walker D., Longhi J., Kirkpatrick R. J. and Hays J. F.(1976b) Differentiation of an Apollo 12 picrite magma. Proc. Lunar Sci. Conf. 7th, p. 1365-1389.

Warner J. L. (1971) Lunar crystalline rocks: Petrology and geology. Proc. Lunar Sci. Conf. 2nd, p. 469-480.

Weill D. F., Grieve R. A., McCallum I. S., Bottinga Y. (1971) Mineralogy-petrology of lunar samples. Microprobe studies of samples 12021 and 12022; viscosity of melts of selected lunar compositions. Proc. Lunar Sci. Conf. 2nd, p. 413-430.

Willis J. P., Ahrens L. H., Dauchin R. V., Erlank A. J., Gurney J. J., Hofmeyr P. K., McCarthy T. S. and Ovren M. J. (1971) Some interelement relationships between lunar rocks and fines and stony meteorites. Proc. Lunar Sci. Conf. 2nd, p. 1123-1138.

Table 1. Cooling Rate Sequence of Apollo 12 Ilmenite Suite Basalts

Porphyritic Basalts (Most Rapid Cooling)	Mg/(Mg+Fe)*
12008	0.500
12045	0.484
12022	-
Medium-Grained Subophitic Basalts	
12047	0.364
12051	-
12054	0.382
12063	-
12056	0.434
Medium-Grained Equigranular Basalt	
12016	0.499
Coarse-Grained Cumulates (Slowest Cooling)	
12036	0.577
12005	0.615

*Mg/(Mg+Fe) data taken from Rhodes et al. (1977)

Table 2. Modal Analyses of Medium and Coarse Grained Ilmenite Suite Basalts

	12047	12051	12063	12056	12016	12036	12005
Olivine	-	-	6.0	10.8	12.0	24	30.0
Pyroxene undif.	-	58.8	60.0	-	-	58	-
Low-Ca Pyroxene	15.0	-	-	20.5	24.1	-	35.5
High-Ca Pyroxene	33.4	-	-	28.7	28.0	-	21.0
Feldspar	38.0	26.5	25.0	28.8	29.1	12	11.0
Ilmenite	5.3	-	-	6.8	4.8	-	1.9
Spinel	1.0	-	2.0	1.6	1.6	-	0.5
Opaques undif.	-	9.3	6.0	-	-	5	-
Silica Phase	5.3	2.8	1.6	0.8	Tr	-	-
Fayalite	-	-	-	1.5	Tr	-	-
Mesostasis undif.	2.0	2.6	5.0	1.0	0.6	-	0.1
Norm. Oliv.	-	-	8.8	6.9	18.2	28.3	42.0
Norm. Q.	2.2	1.1	-	-	-	-	-

Source of Modal Data

12047, 12056, 12016, 12005 - This study
12063 - Average of two values - McGee et al. (1977); Papike et al. (1976)
12051 - Average of two values - Brown et al. (1971); Papike et al. (1976)
12036 - Prinz (1977) personal communication
Normative data calculated from analysis by Rhodes et al. (1977); Willis et al. (1971) and Compston et al. (1971)
Opaques undif. = spinel + troilite + metal + ilmenite
Mesostasis undif. = K-feldspar + silica and potassium-rich glass ± fayalite ± silica phase + phosphate

Table 3. Microprobe Analyses of Olivine

	1	2	3	4	5	6	7	8	9
SiO_2	37.25	35.50	36.62	37.37	28.89	36.75	35.96	35.52	35.78
TiO_2	0.05	0.18	0.05	0.06	0.13	0.04	0.49	0.10	0.09
Al_2O_3	0.00	0.00	0.00	0.00	0.00	0.00	0.03	0.03	0.02
Cr_2O_3	0.33	0.23	0.13	0.29	0.01	0.16	0.07	0.09	0.11
FeO	25.27	35.90	29.02	24.93	64.00	29.64	34.67	36.66	34.75
MnO	0.25	0.30	0.34	0.26	0.63	0.28	0.33	0.36	0.34
MgO	35.76	26.75	32.92	35.94	3.13	33.13	29.11	27.59	28.58
CaO	0.29	0.43	0.25	0.30	0.61	0.28	0.18	0.28	0.26
Total	99.20	99.29	99.33	99.15	98.40	100.27	100.84	100.62	99.92
Si	0.944	0.999	0.994	0.996	1.002	0.990	0.987	0.989	0.993
Ti	0.001	0.004	0.001	0.001	0.003	0.001	0.010	0.002	0.002
Al	0.000	0.000	0.000	0.000	0.000	0.000	0.001	0.001	0.000
Cr	0.007	0.005	0.003	0.006	0.000	0.003	0.002	0.002	0.003
Fe	0.564	0.845	0.659	0.555	1.794	0.668	0.796	0.853	0.807
Mn	0.006	0.007	0.008	0.006	0.018	0.006	0.008	0.009	0.008
Mg	1.422	1.122	1.332	1.427	0.156	1.330	1.192	1.144	1.183
Ca	0.008	0.013	0.007	0.009	0.022	0.008	0.005	0.008	0.008
Total	3.002	2.995	3.004	3.000	2.995	3.007	3.001	3.008	3.003
Fo	71.6	57.0	66.9	72.0	8.0	66.6	60.0	57.3	59.4
Fa	28.4	43.0	33.1	28.0	92.0	33.4	40.0	42.7	40.6

1. 12008 - most magnesian core composition.
2. 12008 - most iron-rich rim composition.
3. 12016 - most magnesian composition analyzed. Core of anomalously large grain.
4. 12056 - most magnesian composition. Core of large grain.
5. 12056 - fayalite crystallized from iron-rich immiscible fraction of residual mesostasis.
6. 12005 - core of very large grain.
7. 12005 - rim of euhedral grain partly enclosed in a poikilitic ilmenite grain within "interstitial" assemblage.
8. 12005 - core of the same grain.
9. 12005 - rim of euhedral grain adjacent to plagioclase in the "interstitial" assemblage.

Table 4. Microprobe Analyses of Spinel

	1	2	3	4	5	6	7	8	9
TiO_2	9.49	6.02	8.44	24.77	7.80	27.40	9.95	27.06	7.27
Al_2O_3	11.41	12.27	10.51	4.51	10.11	3.30	10.66	3.68	11.36
Cr_2O_3	38.40	45.78	41.19	13.30	39.49	11.83	37.57	12.59	43.11
FeO	34.54	28.13	32.93	53.80	39.75	55.51	35.27	53.43	32.31
MnO	0.72	0.68	0.80	0.64	0.54	0.44	0.54	0.40	0.58
MgO	4.66	7.20	5.26	1.74	0.81	0.74	4.21	1.69	4.90
CaO	0.09	0.05	0.11	0.29	0.00	0.06	0.08	0.07	0.04
Total	99.31	100.13	99.23	99.06	98.50	99.27	98.27	98.92	99.57
Ti	1.961	1.209	1.746	5.447	1.687	6.048	2.087	5.934	1.495
Al	3.693	3.860	3.409	1.553	3.424	1.140	3.507	1.264	3.661
Cr	8.337	9.657	8.961	3.075	8.972	2.744	8.289	2.901	9.323
Fe	7.933	6.278	7.579	13.156	9.555	13.626	8.232	13.028	7.391
Mn	0.168	0.153	0.186	0.160	0.132	0.108	0.127	0.098	0.134
Mg	1.906	2.864	2.158	0.757	0.345	0.325	1.749	0.736	1.998
Ca	0.025	0.014	0.031	0.090	0.000	0.018	0.022	0.023	0.020
Total	24.024	24.033	24.069	24.239	24.115	24.010	24.015	23.984	24.014
Cr/(Cr+Al)	0.693	0.714	0.724	0.664	0.724	0.706	0.703	0.697	0.718
Fe/(Fe+Mg)	0.806	0.687	0.778	0.946	0.965	0.977	0.825	0.947	0.787

n.d. - not analyzed for

1. 12008 - relatively titanium-rich rim of euhedral spinel in groundmass.
2. 12008 - most refractory core composition analyzed.
3. 12045 - typical core of spinel enclosed within olivine phenocryst.
4. 12045 - chromian ulvöspinel rim in groundmass.
5. 12056 - low-Mg core of mantled grain
6. 12056 - low-Mg ulvöspinel adjacent to residual mesostasis
7. 12056 - high-Mg core of a relatively unzoned spinel in the core of a pyroxene grain.
8. 12056 - chromian ulvöspinel rim on chromian spinel, all enclosed in a pyroxene grain.
9. 12056 - high-Mg chromian spinel.

Table 4. Microprobe Analyses of Spinel - concluded

	10	11	12	13	14	15	16	17	18
TiO_2	25.87	8.68	28.23	8.39	6.64	21.36	6.78	24.47	1.78
Al_2O_3	4.52	11.29	3.35	10.72	11.75	5.32	12.03	5.39	45.98
Cr_2O_3	14.38	40.26	8.90	45.17	42.88	24.47	44.21	19.03	17.81
FeO	50.91	35.46	57.33	32.55	32.41	44.26	28.69	44.69	23.67
MnO	0.53	0.52	0.52	0.31	0.32	0.36	0.27	0.34	0.14
MgO	2.92	3.63	1.15	3.62	4.06	3.71	6.45	5.14	10.07
CaO	0.04	0.05	0.01	n.d.	n.d.	n.d.	n.d.	n.d.	n.d.
Total	99.17	99.88	99.49	100.75	98.05	99.48	98.43	99.06	99.45
Ti	5.590	1.797	6.230	1.712	1.389	4.534	1.388	5.156	0.306
Al	1.530	3.660	1.159	3.424	3.853	1.768	3.853	1.778	12.385
Cr	3.268	8.757	2.065	9.684	9.432	5.459	9.500	4.214	3.218
Fe	12.233	8.158	14.069	7.382	7.539	10.444	6.522	10.471	4.525
Mn	0.128	0.121	0.129	0.070	0.074	0.086	0.062	0.081	0.026
Mg	1.250	1.487	0.504	1.462	1.683	1.560	2.611	2.148	3.432
Ca	0.014	0.014	0.002	—	—	—	—	—	—
Total	24.012	23.995	24.158	23.734	23.969	23.852	23.936	23.848	23.892
Cr/(Cr+Al)	0.681	0.705	0.641	0.739	0.710	0.755	0.711	0.703	0.206
Fe/(Fe+Mg)	0.907	0.846	0.965	0.835	0.818	0.870	0.714	0.830	0.569

10. 12016 - high-Mg chromian ulvöspinel
11. 12016 - low-Mg chromian spinel
12. 12016 - low-Mg chromian ulvöspinel
13. 12005 - chromian spinel intergrown with reduced ilmenite
14. 12005 - typical chromian spinel enclosed in olivine
15. 12005 - chromian ulvöspinel also included in olivine
16. 12005 - typical chromian spinel enclosed in the core of a pyroxene
17. 12005 - chromian ulvöspinel enclosed in the rim of a pyroxene
18. 12005 - single grain of Cr-aluminum pleonaste in pyroxene

Table 5. Microprobe Analyses of Pyroxene

	1	2	3	4	5	6	7	8	9
SiO_2	43.14	41.68	46.50	46.00	49.72	50.15	50.45	50.65	48.18
TiO_2	5.17	7.44	2.86	0.96	1.66	1.16	1.50	0.70	0.79
Al_2O_3	7.67	9.02	4.73	1.44	3.38	2.30	2.83	0.78	1.09
Cr_2O_3	1.03	0.55	0.20	0.06	0.89	0.72	0.80	0.20	0.17
FeO	16.79	13.26	18.98	40.09	13.18	17.76	15.30	25.89	33.50
MnO	0.29	0.20	0.38	0.66	0.26	0.31	0.22	0.38	0.45
MgO	10.13	8.29	8.89	2.47	16.27	19.80	16.62	15.78	8.85
CaO	15.08	18.64	16.73	7.81	13.84	6.89	11.92	5.00	6.24
Na_2O	0.08	0.15	0.03	0.01	0.06	0.01	0.00	0.00	0.01
Total	99.38	99.23	99.30	99.51	99.26	99.10	99.64	99.39	99.27
Si	1.676	1.615	1.820	1.941	1.872	1.893	1.896	1.963	1.954
Ti	0.151	0.217	0.084	0.031	0.047	0.033	0.043	0.002	0.024
Al^{IV}	0.324	0.385	0.180	0.059	0.128	0.102	0.104	0.036	0.046
Al^{VI}	0.027	0.027	0.038	0.013	0.022	0.000	0.021	0.000	0.006
Cr	0.032	0.017	0.006	0.002	0.027	0.022	0.024	0.006	0.006
Fe	0.545	0.429	0.621	0.414	0.415	0.560	0.481	0.839	1.136
Mn	0.010	0.007	0.013	0.023	0.008	0.010	0.007	0.012	0.015
Mg	0.587	0.479	0.519	0.155	0.913	1.114	0.931	0.912	0.535
Ca	0.628	0.774	0.701	0.353	0.558	0.279	0.480	0.208	0.271
Na	0.006	0.011	0.003	0.001	0.004	0.000	0.000	0.000	0.001
Total	3.985	3.960	3.985	3.992	3.995	4.013	3.987	3.996	3.993
Wo	35.7	46.0	38.1	18.4	29.6	14.3	25.4	10.6	14.0
En	33.3	28.5	28.2	88.1	48.4	57.0	49.2	46.5	27.5
Fs	31.0	25.5	33.7	73.6	22.0	28.7	25.4	42.8	58.5

1. 12008 - dendritic microphenocryst.
2. 12045 - core of brown phenocryst.
3. 12045 - rim of same phenocryst.
4. 12045 - rim of pale green groundmass pyroxene.
5. 12016 - augite core of large grain.
6. 12016 - low-calcium pyroxene intergrown with augite in the core of same large grain.
7. 12016 - subcalcic augite in the core of another large grain.
8. 12016 - low-clacium rim.
9. 12016 - iron-rich, low-calcium grain margin adjacent to mesostasis.

Table 5 .Microprobe Analyses of Pyroxene - continued

	10	11	12	13	14	15	16	17	18
SiO_2	49.56	51.74	51.10	49.82	45.87	50.53	52.33	51.21	49.90
TiO_2	1.97	1.16	1.41	1.18	1.00	1.61	0.90	0.83	1.77
Al_2O_3	3.40	2.27	2.54	2.17	1.66	3.22	1.64	1.04	2.52
Cr_2O_3	0.94	0.60	0.68	0.25	0.21	0.86	0.71	0.32	0.60
FeO	12.05	17.68	15.33	24.27	35.49	10.72	15.71	20.10	13.37
MnO	0.24	0.29	0.26	0.36	0.43	0.23	0.31	0.38	0.22
MgO	15.09	19.05	17.42	13.23	3.44	16.26	21.80	20.35	16.12
CaO	16.23	7.15	10.46	7.95	11.13	16.47	6.81	5.32	15.20
Na_2O	0.04	0.06	0.02	0.04	0.08	0.07	0.00	0.03	0.07
Total	99.52	100.00	99.22	99.26	99.31	99.97	100.20	99.58	99.78
Si	1.866	1.927	1.918	1.936	1.916	1.879	1.927	1.931	1.878
Ti	0.056	0.033	0.040	0.035	0.032	0.045	0.025	0.024	0.050
Al^{IV}	0.134	0.073	0.082	0.064	0.082	0.121	0.071	0.046	0.112
Al^{VI}	0.016	0.027	0.030	0.035	0.000	0.020	0.000	0.000	0.000
Cr	0.028	0.018	0.020	0.008	0.007	0.025	0.021	0.010	0.018
Fe	0.379	0.551	0.481	0.789	1.240	0.333	0.484	0.634	0.421
Mn	0.008	0.009	0.008	0.012	0.015	0.007	0.010	0.012	0.007
Mg	0.846	1.057	0.973	0.766	0.214	0.902	1.196	1.144	0.904
Ca	0.654	0.285	0.421	0.331	0.498	0.656	0.269	0.215	0.613
Na	0.003	0.004	0.002	0.003	0.007	0.005	0.000	0.002	0.005
Total	3.991	3.984	3.977	3.977	4.011	3.995	4.002	4.018	4.009
Wo	34.8	15.1	22.4	17.5	25.5	35.0	14.0	10.9	32.0
En	45.0	55.8	51.9	40.6	11.0	48.5	61.2	57.1	47.0
Fs	20.2	29.1	25.7	41.9	63.5	17.5	24.8	32.0	22.0

10. 12056 - augite in core of large grain.
11. 12056 - relatively rare low-calcium pyroxene in core of large grain.
12. 12056 - sub-calcic augite in core of large grain.
13. 12056 - rim adjacent to core of same grain — marks an abrupt shift in composition.
14. 12056 - ferroaugite margin adjacent to mesostasis.
15. 12005 - augite core of large grain.
16. 12005 - low-calcium pyroxene in core of large grain.
17. 12005 - relatively iron-rich, low-calcium margin.
18. 12005 - relatively iron-rich augite margin.

Table 6. Microprobe Analyses of Feldspar

	1	2	3	4	5	6	7	8	9
SiO_2	46.75	49.28	50.18	47.68	48.34	47.95	45.51	50.33	66.40
TiO_2	0.09	0.04	0.10	0.11	0.05	0.04	0.08	0.10	0.23
Al_2O_3	33.59	31.06	30.89	32.70	32.40	32.24	35.16	31.41	18.74
FeO	0.49	1.48	1.11	0.80	1.25	1.84	0.33	0.56	0.45
MgO	0.30	0.07	0.08	0.37	0.06	0.01	0.19	0.10	0.00
CaO	17.39	15.90	15.15	17.02	16.64	16.91	18.42	14.41	0.27
Na_2O	0.97	1.23	1.65	1.24	1.11	0.85	0.76	2.27	0.59
K_2O	0.06	0.58	0.61	0.07	0.24	0.54	0.06	1.02	15.19
BaO	0.00	0.13	0.07	0.00	0.00	0.10	n.d.	n.d.	n.d.
Total	99.60	99.75	99.85	100.00	100.08	100.49	100.49	100.20	101.87
Si	2.155	2.271	2.301	2.192	2.220	2.206	2.088	2.297	2.997
Ti	0.003	0.001	0.004	0.-04	0.002	0.001	0.003	0.004	0.008
Al	1.827	1.687	1.670	1.772	1.754	1.748	1.901	1.689	0.997
Fe	0.019	0.057	0.043	0.031	0.048	0.071	0.013	0.021	0.017
Mg	0.021	0.005	0.006	0.025	0.004	0.001	0.013	0.007	0.000
Ca	0.860	0.785	0.744	0.838	0.819	0.834	0.905	0.705	0.013
Na	0.086	0.110	0.147	0.111	0.098	0.076	0.067	0.201	0.051
K	0.003	0.034	0.036	0.004	0.014	0.032	0.003	0.059	0.874
Ba	0.000	0.002	0.001	0.000	0.000	0.002	—	—	—
Total	4.973	4.953	4.951	4.976	4.958	4.970	4.994	4.985	4.959
An	90.6	84.5	80.3	87.9	88.0	88.5	92.8	73.1	1.4
AG	9.1	11.8	15.9	11.6	10.5	8.1	6.9	20.8	5.4
Or	0.3	3.7	3.9	0.5	1.5	3.4	0.3	6.1	93.2

n.d. - not analyzed for

1. 12016 - core of large equant grain with typical high An, low Fe/Fe+Mg.
2. 12016 - rim adjacent to mesostasis.
3. 12016 - rim adjacent to pyroxene.
4. 12056 - core of large equant grain.
5. 12056 - rim near mesostasis patch.
6. 12056 - rim near mesostasis patch.
7. 12005 - core of large equant grain with high An and low Fe/Fe+Mg.
8. 12005 - sodic bytownite intergrown with potassium feldspar.
9. 12005 - K-feldspar in holocrystalline patch of mesostasis.

FIGURE CAPTIONS

Figure 1: Photomicrographs of porphritic basalts. (a) Vitrophyre 12008: Glomerophyric aggregates of olivine phenocrysts and skeletal chain-like olivine microphenocrysts set in a fine-grained groundmass. (b) Reflected light detail of phenocryst and groundmass relations in 12008. Left - olivine phenocryst with small spinel octahedra included in rim. Right - feathery augite dendrite (px). Note very fine-grained filamental ilmenite in matrix. (c) 12045: Olivine phenocrysts (white) are rimmed by aluminous titanaugite (gray). Cigar-shaped phenocrysts of compositionally equivalent augite are set in a variolitic groundmass of pyroxene, plagioclase, a silica phase and ilmenite. (d) Reflected light detail of augite phenocrysts and variolitic groundmass in 12045. Note parallelism of skeletal ilmenite plates.

Figure 2: Photomicrographs of medium-grained basalts. (a) 12016 (b, c) 12016 - Reflected and transmitted light details of an anomalously large mesostasis segregation in upper right of (a). The large, light gray grains are ilmenite. Other well crystallized phases are irregular grains of fayalite (Fa) and silica (Si). Matrix consists of devitrified(?) Si+K-rich glass, phosphate and feldspar. (d) 12056 - Same scale as (a). (e, f). Reflected light details of mesostasis segregations in 12056.

Figure 3: Camera Lucida tracing of 12005,13. Individual large pyroxene grains are indicated by parallelism of hachures. "Opaques" includes spinel, metal, troilite and small ilmenite grains.

Figure 4: Photomicrographs of 12005. All with partially crossed nicols: a-c-d same scale, b-d-f same scale (a). Abundant euhedral to subhedral olivines poikilitically enclosed in plagioclase. (b) Detail of same area. (c) Twinned pyroxene oikocryst. Numerous grains of anhedral olivine and euhedral spinel are included. (d) Detail of upper left portion of c. Twin planes run horizontally. Augite core is at the top, rim and grain boundary with mesostasis segregations (triangular shape) are at the base. (e) Right - an anomalously large olivine grain containing abundant melt inclusions. Upper left - elongate olivine grain in optical continuity with large grain. (f) Ilmenite oikocryst enclosing olivine and pyroxene.

Figure 5: Reflected light photomicrographs of oxide and mesostasis assemblages in 12005. All at same scale. (a) Metal droplet (m) inclusion in chromian spinel. (b) Holocrystalline segregation of mesostasis surrounded by pyroxene (see 4d). K-feldspar (k), ilmenite (i), metal and troilite (m, t), and acicular phosphate (p) included in plagioclase. (c) Spinel (s) and rutile (r) formed by subsolidus reduction of ilmenite (ilm). Reduction is best developed adjacent to small segregations of mesostasis which include metal and troilite. (d) Ilmenite (i) reduction lamellae in ulvöspinel (usp) with fine-grained intergrown metal and troilite.

Figure 6: Microprobe analyses of olivines. Fo-content vs. Cr_2O_3 for olivine more magnesian than Fo_{37}.

Figure 7: Microprobe analyses of spinel in 12008, 12045, 12056 and 12016. Normalized compositions are plotted on normalized Ti:Cr:Al (top) and Cr:Fe:Mg(bottom) ternaries. Analyses from 12008 (+) and 12045 (0) are plotted together.

Figure 8: Microprobe analyses of spinel in 12005. (a) Analyses plotted along the Usp-Cr join and (b) on the normalized Cr:Fe:Mg and Ti:Cr:Al ternaries.

Figure 9: Microprobe traverse illustrating zoning in a single grain of chromian spinel in 12005.

Figure 10: Microprobe analyses of pyroxenes plotted in terms of quadrilateral components.

Figure 11: Microprobe analyses of pyroxenes illustrating variations in Ti-Al relations. 12022 trend after Bence and Papike (1972).

Figure 12: Microprobe analyses of pyroxenes. Cr_2O_3 vs. Fe/(Fe+Mg). Note different scales for Fe/(Fe+Mg).

Figure 13: Microprobe analyses of plagioclase. An-content (a) and K_2O (b) vs. Fe/(Fe+Mg).

Figure 14: Microprobe analyses of ilmenite in 12045, 12016, 12056 and 12005. Cr_2O_3, FeO and TiO_2 vs. MgO.

Figure 15: Microprobe analyses of metal grains in 12005, 12016 and 12056 (Ni vs. CO).

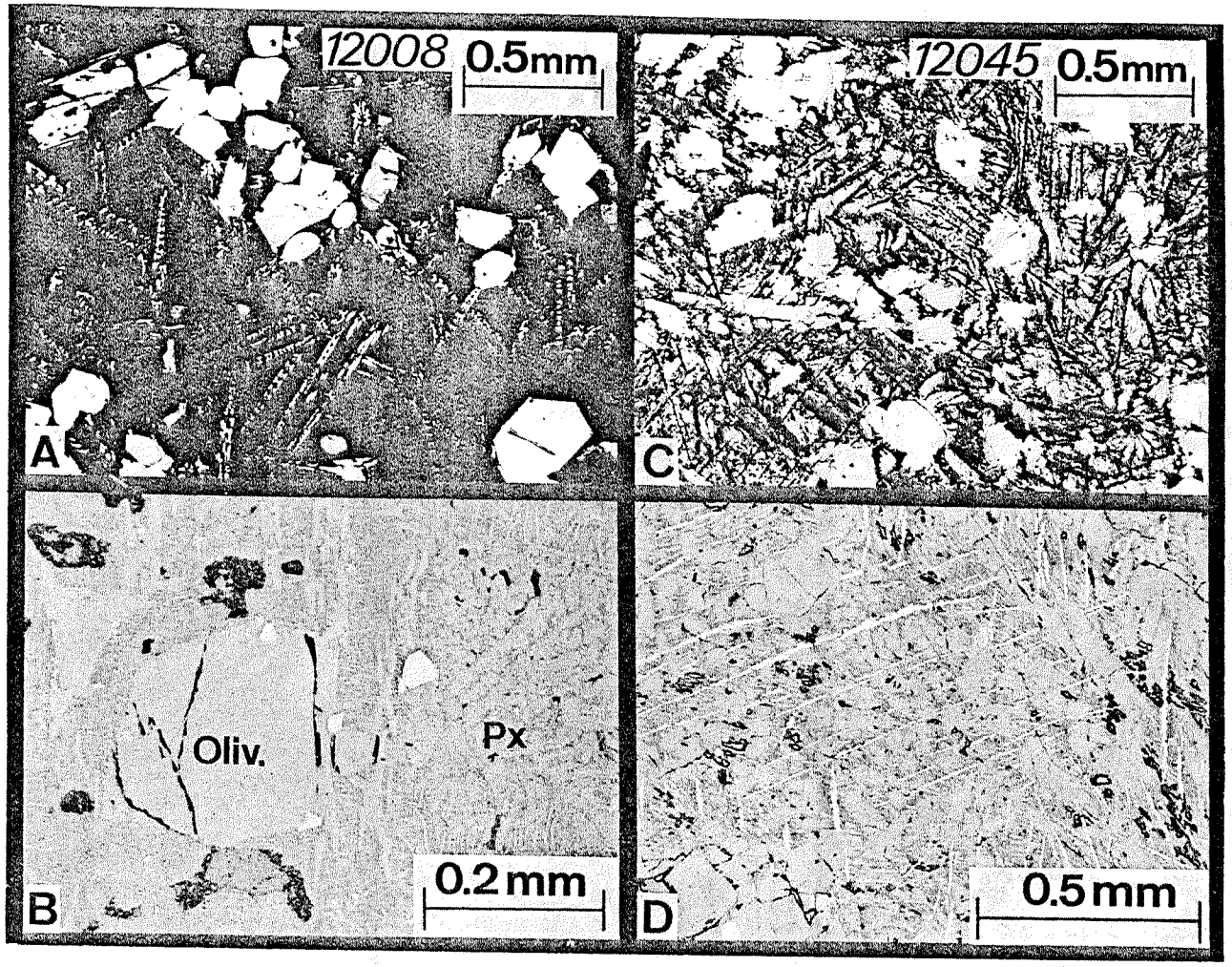

Figure 1

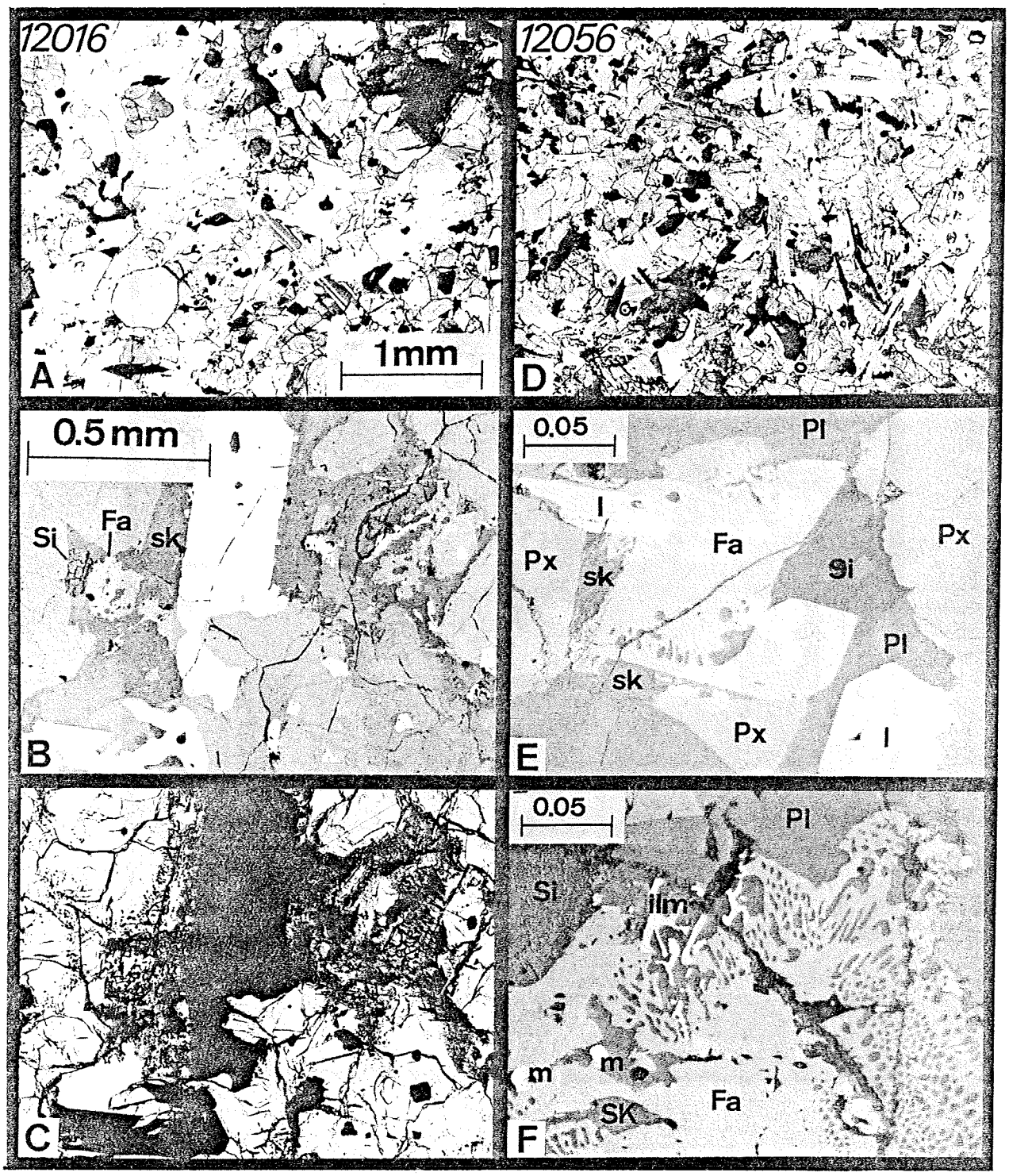
12016
1mm
A
12056
D
0.5 mm
Si
Fa
sk
B
0.05
Pl
l
Px
Fa
sk
Si
Px
Pl
sk
Px
l
E
C
0.05
Pl
Si
ilm
m
m
Fa
SK
F

Figure 2

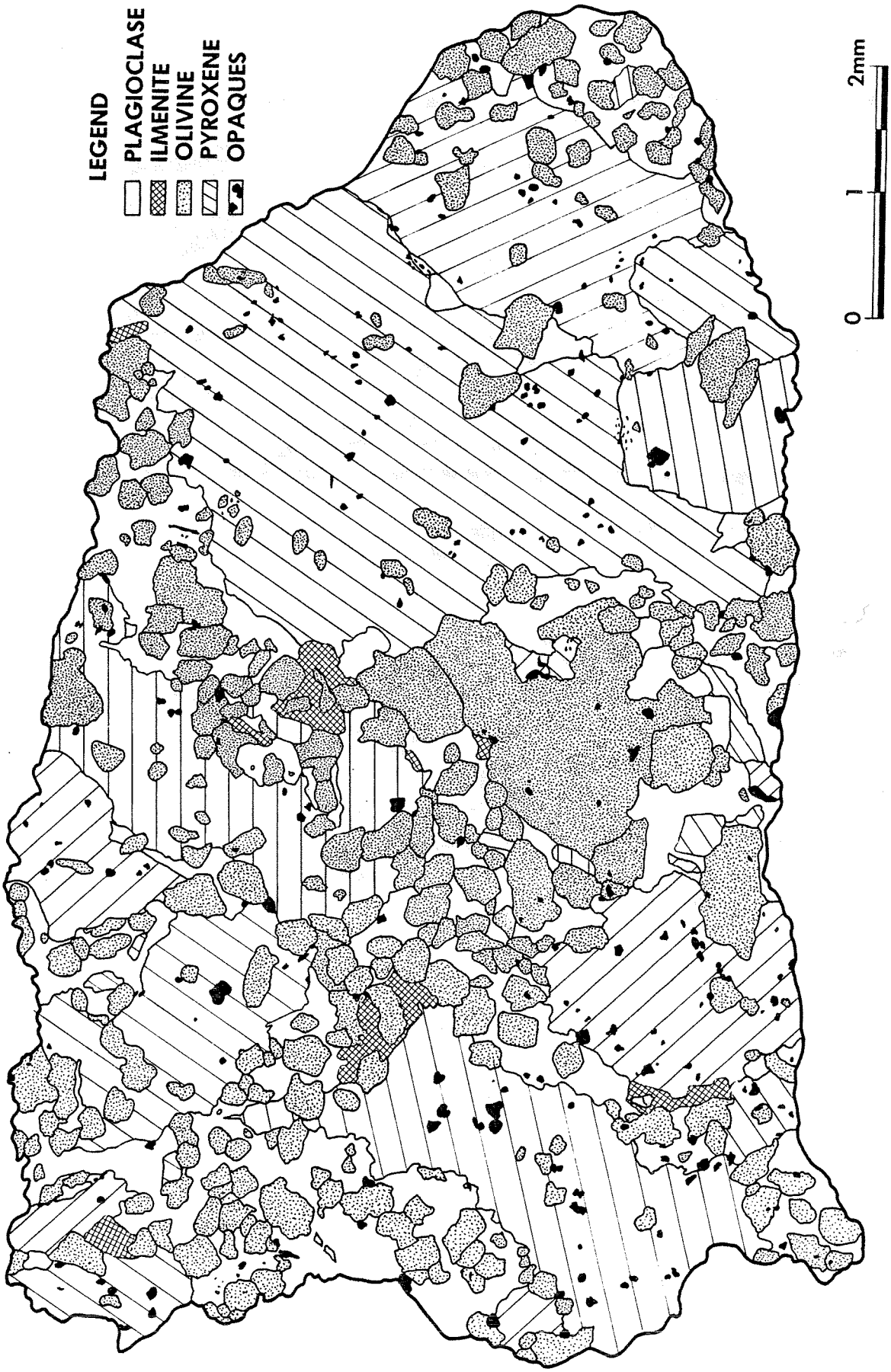
LEGEND
PLAGIOCLASE
ILMENITE
OLIVINE
PYROXENE
OPAQUES
0
1
2mm

FIGURE 3

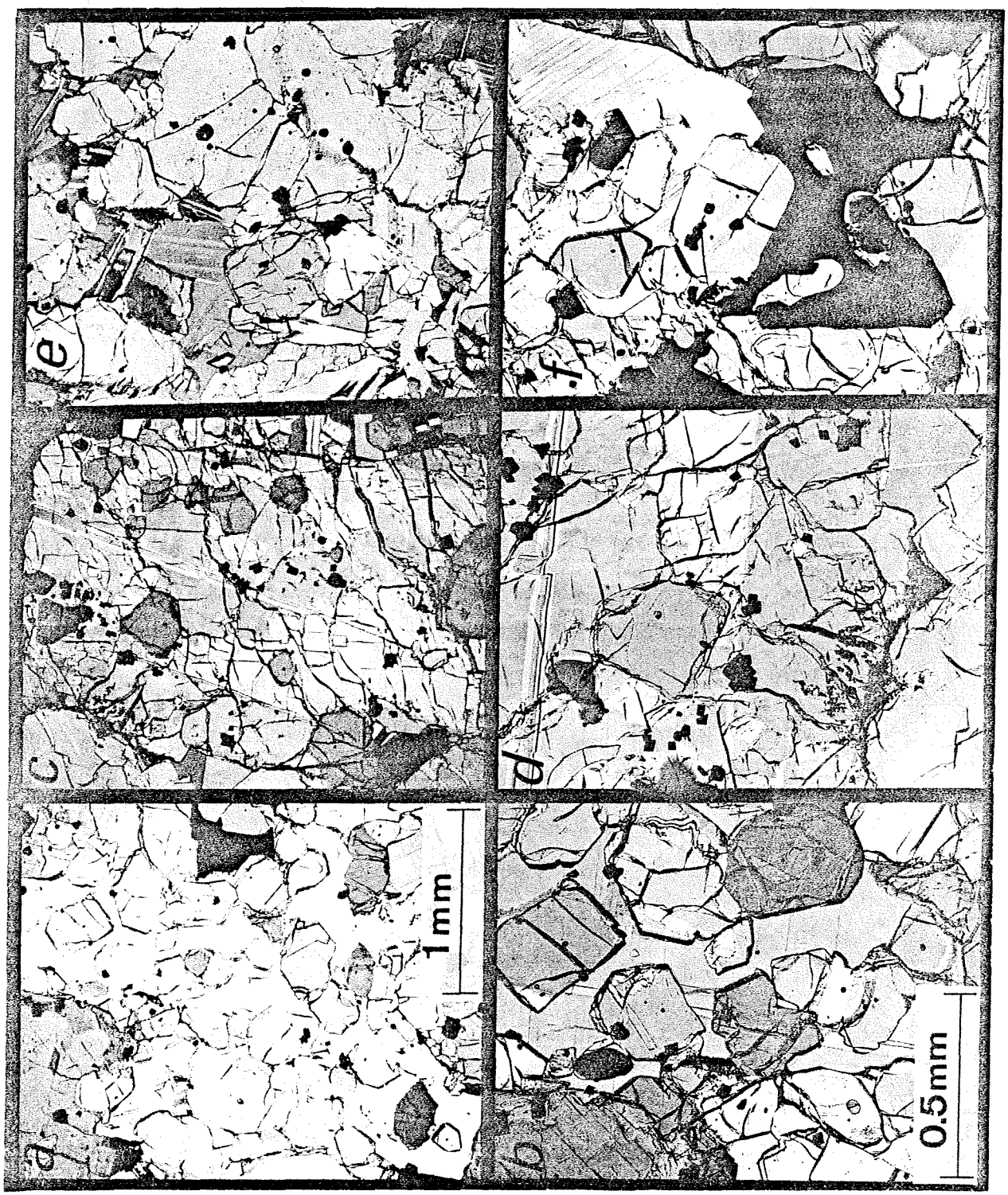

FIGURE 4

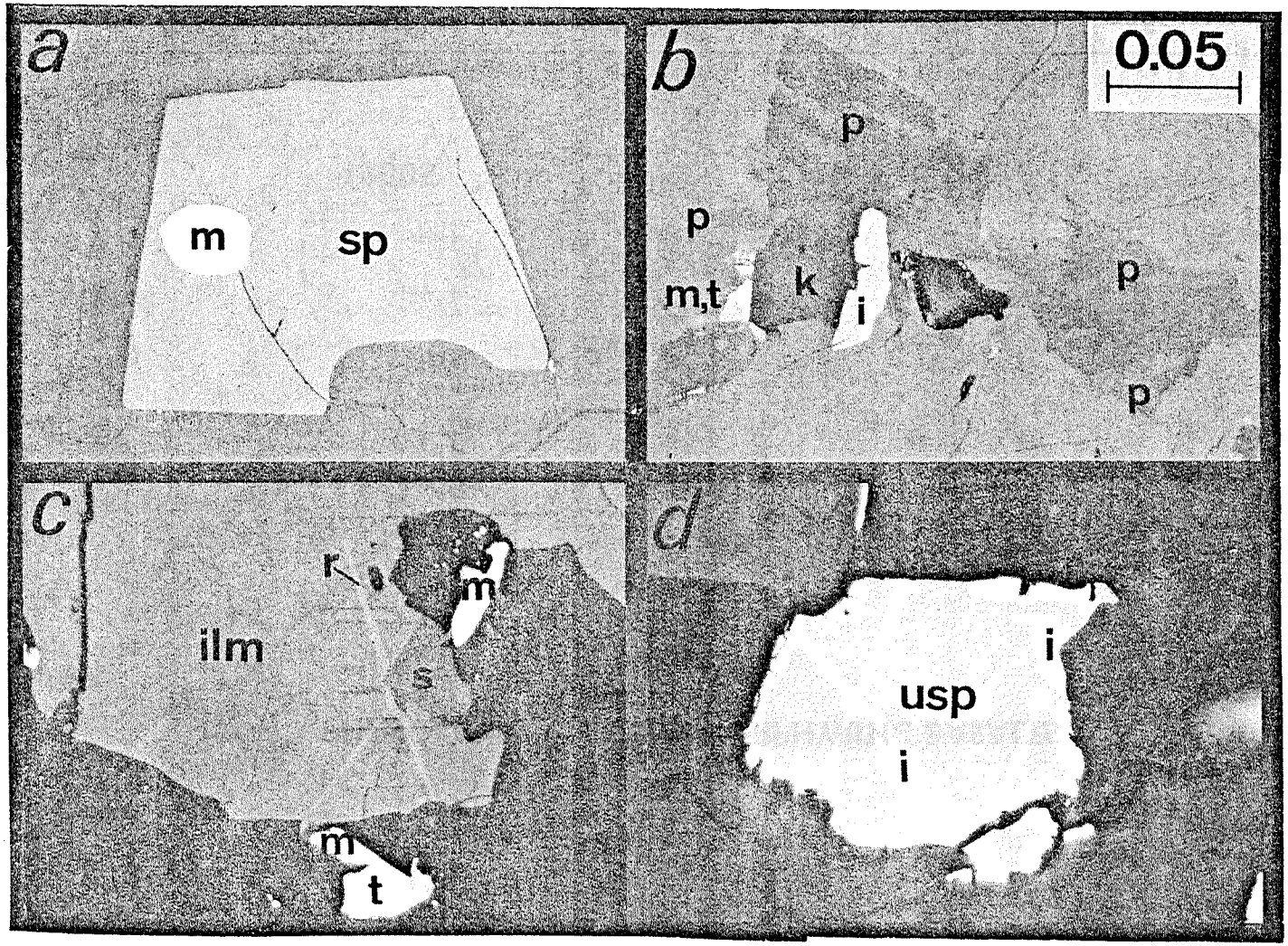

Figure 5

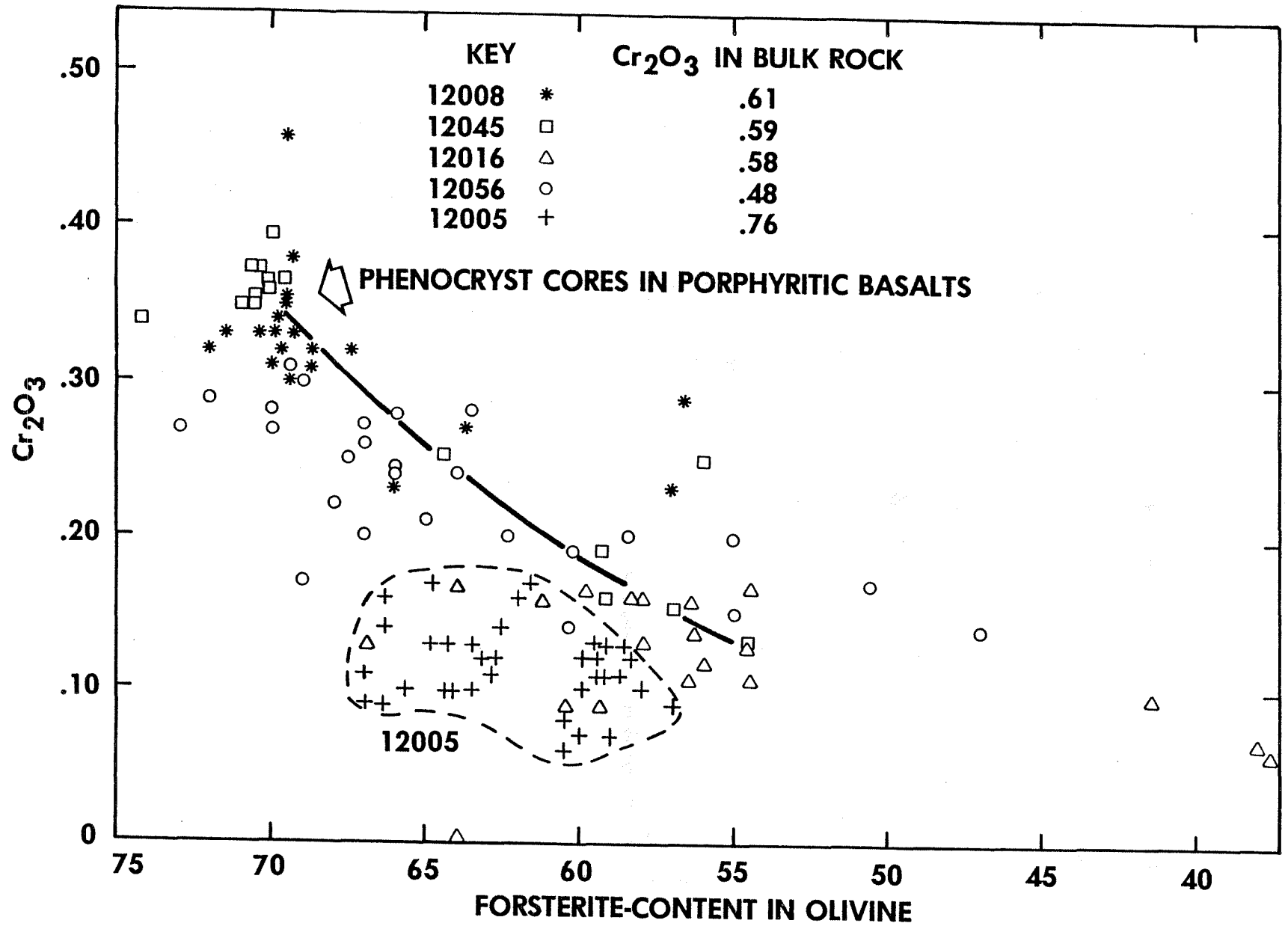
KEY
Cr_2O_3 IN BULK ROCK
12008 * .61
12045 □ .59
12016 △ .58
12056 ○ .48
12005 + .76
PHENOCRYST CORES IN PORPHYRITIC BASALTS
12005
Cr_2O_3
.50
.40
.30
.20
.10
0
75
70
65
60
55
50
45
40
FORSTERITE-CONTENT IN OLIVINE

Figure 6

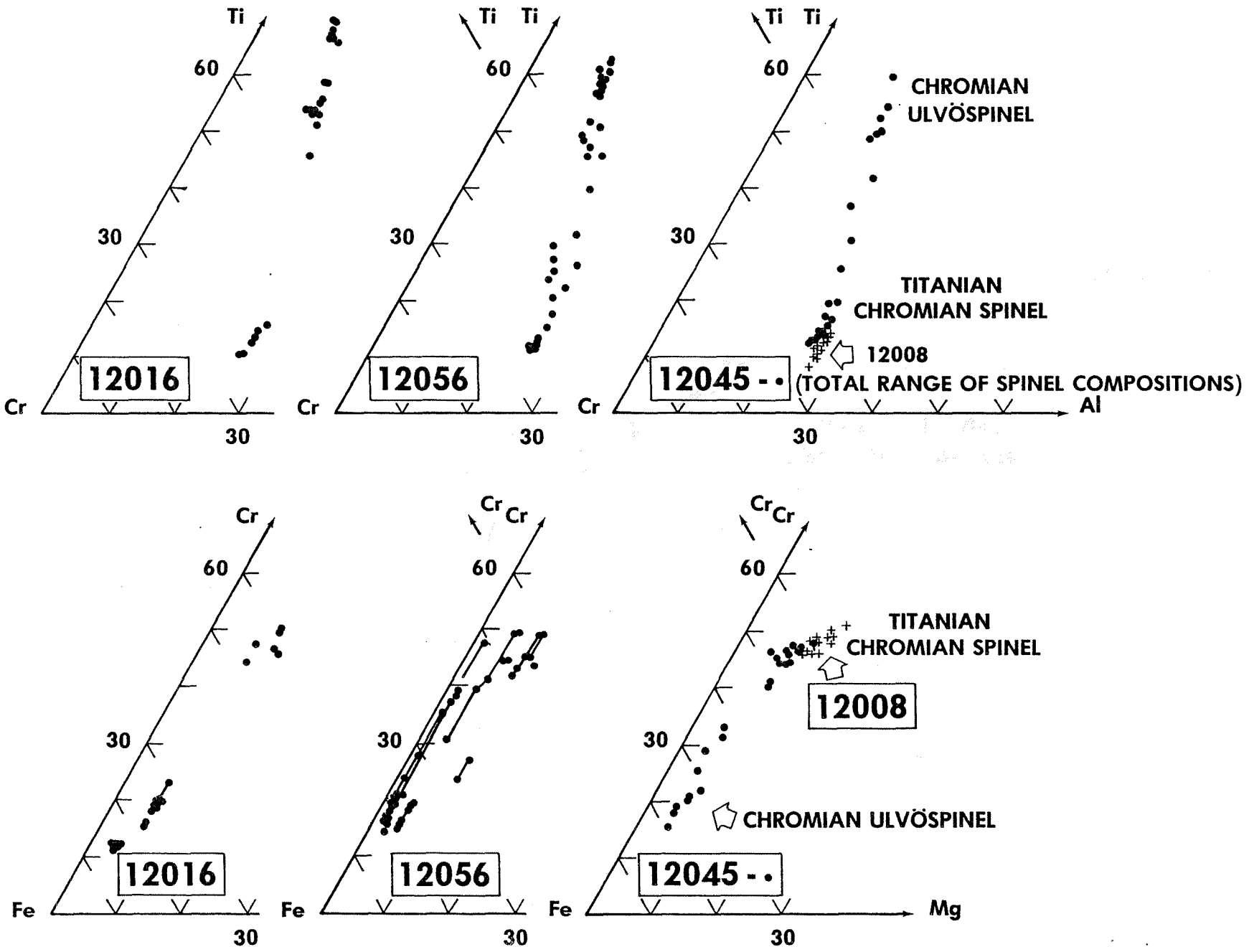
Ti
60
30
Cr
30
12016
Ti Ti
12056
CHROMIAN
ULVÖSPINEL
TITANIAN
CHROMIAN SPINEL
12008
12045 - •
(TOTAL RANGE OF SPINEL COMPOSITIONS)
Al
Cr
Cr Cr
Fe
Mg
TITANIAN
CHROMIAN SPINEL
CHROMIAN ULVÖSPINEL

Figure 7

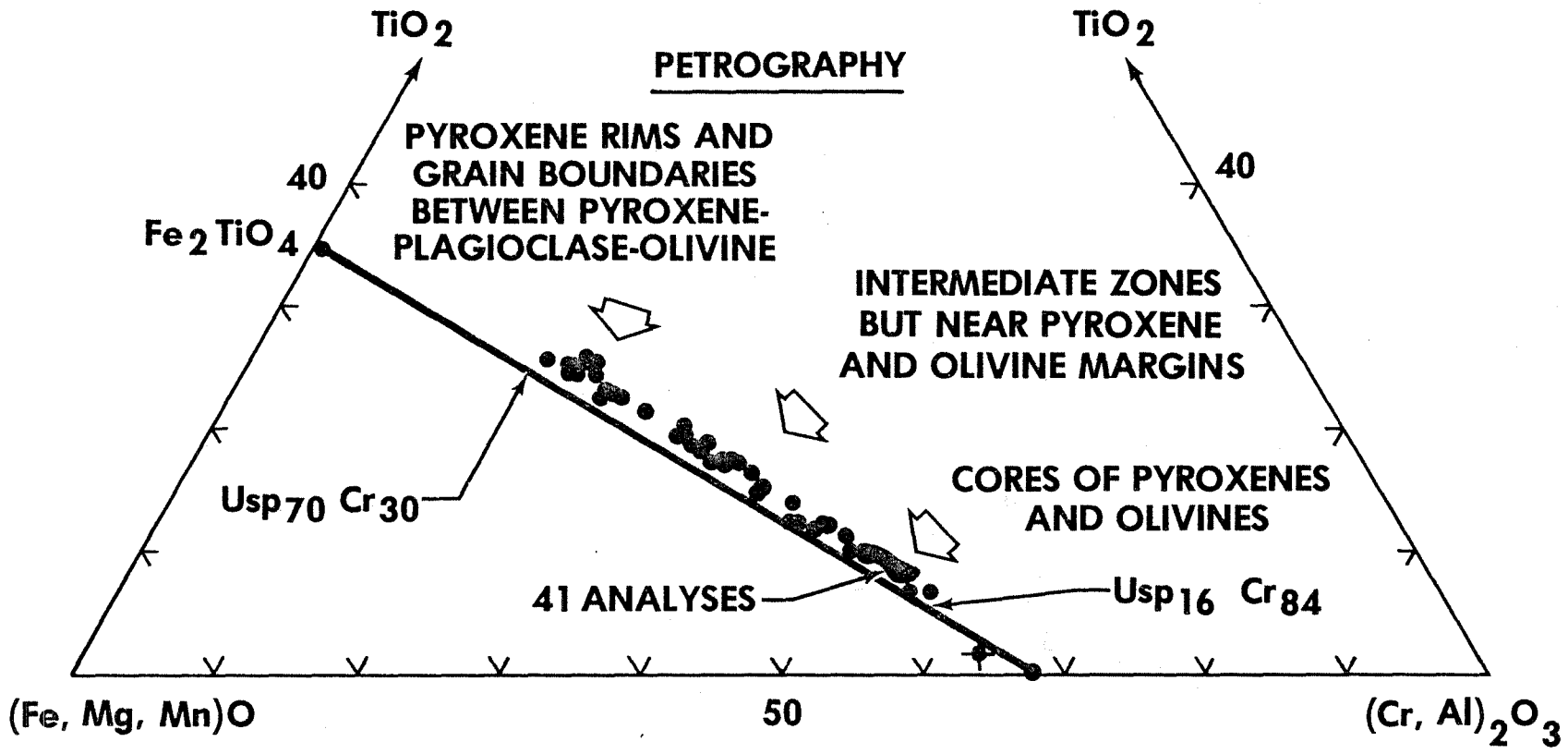
TiO2
PETROGRAPHY
TiO2
PYROXENE RIMS AND
GRAIN BOUNDARIES
BETWEEN PYROXENE-
PLAGIOCLASE-OLIVINE
40
40
Fe2TiO4
INTERMEDIATE ZONES
BUT NEAR PYROXENE
AND OLIVINE MARGINS
Usp70 Cr30
CORES OF PYROXENES
AND OLIVINES
41 ANALYSES
Usp16 Cr84
(Fe, Mg, Mn)O
50
(Cr, Al)2O3

Figure 8a

Figure 8b

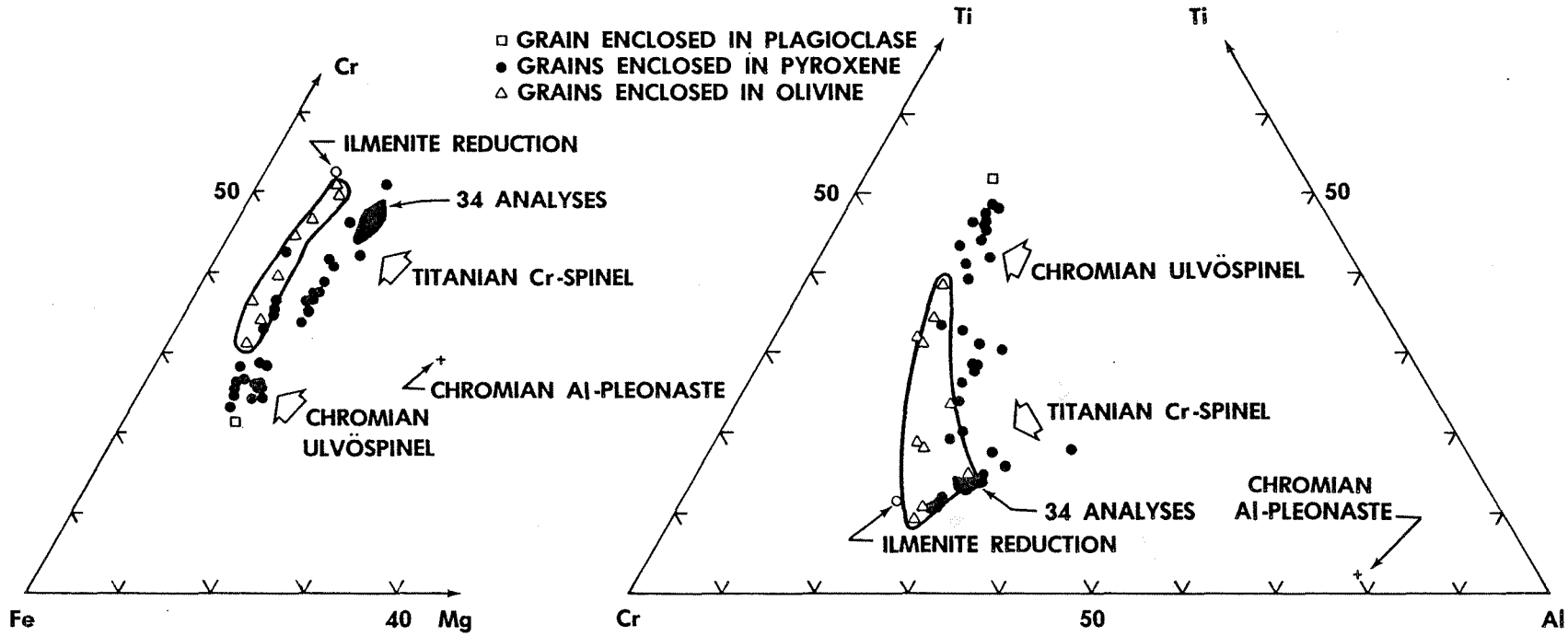
□ GRAIN ENCLOSED IN PLAGIOCLASE
● GRAINS ENCLOSED IN PYROXENE
△ GRAINS ENCLOSED IN OLIVINE
Cr
50
ILMENITE REDUCTION
34 ANALYSES
TITANIAN Cr-SPINEL
CHROMIAN Al-PLEONASTE
CHROMIAN ULVÖSPINEL
Fe
40 Mg
Ti
50
CHROMIAN ULVÖSPINEL
TITANIAN Cr-SPINEL
34 ANALYSES
CHROMIAN Al-PLEONASTE
ILMENITE REDUCTION
Cr
50
Al

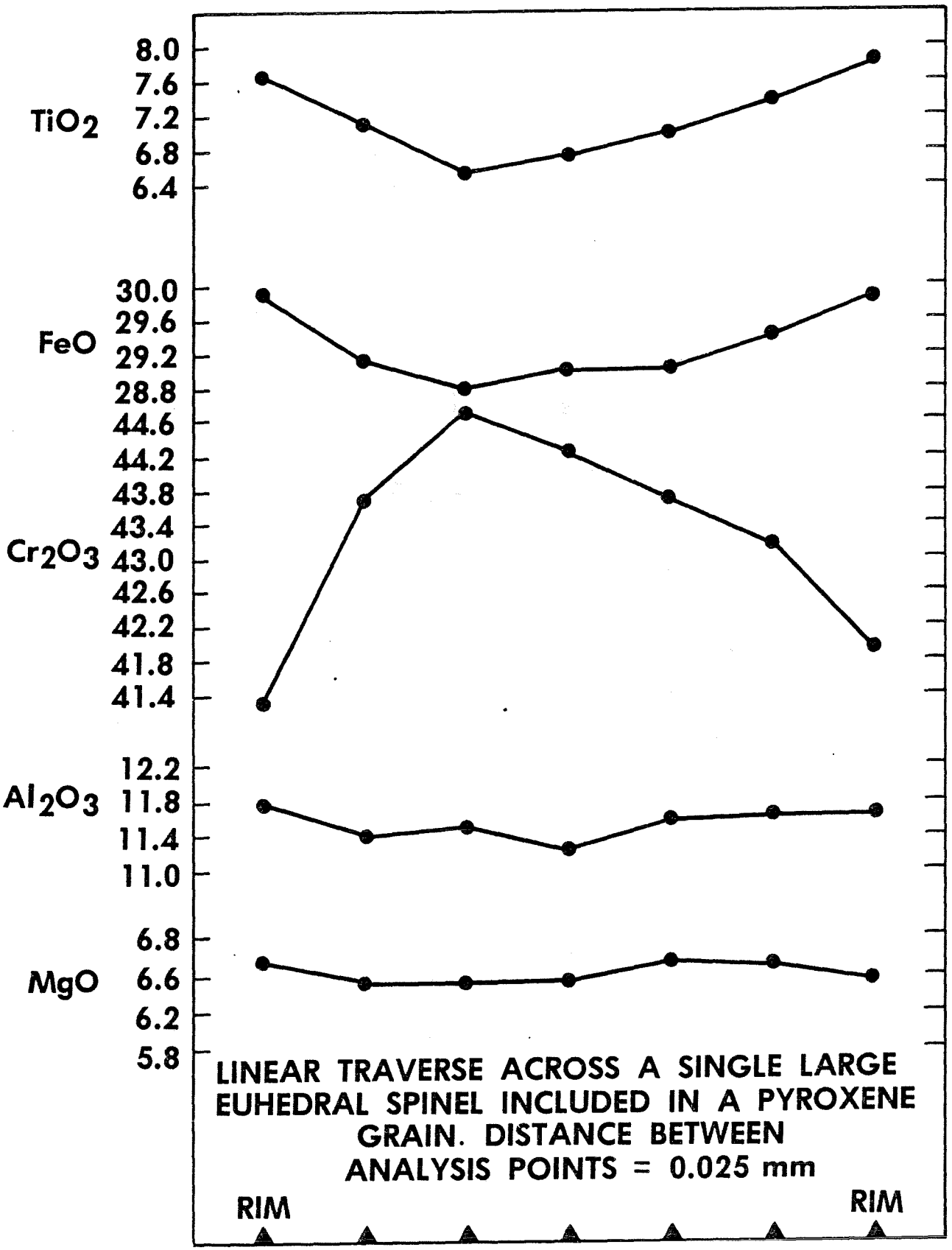
8.0
7.6
TiO2 7.2
6.8
6.4
30.0
29.6
FeO 29.2
28.8
44.6
44.2
43.8
43.4
Cr2O3 43.0
42.6
42.2
41.8
41.4
12.2
Al2O3 11.8
11.4
11.0
6.8
MgO 6.6
6.2
5.8
LINEAR TRAVERSE ACROSS A SINGLE LARGE EUHEDRAL SPINEL INCLUDED IN A PYROXENE GRAIN. DISTANCE BETWEEN ANALYSIS POINTS = 0.025 mm
RIM
RIM

Figure 9

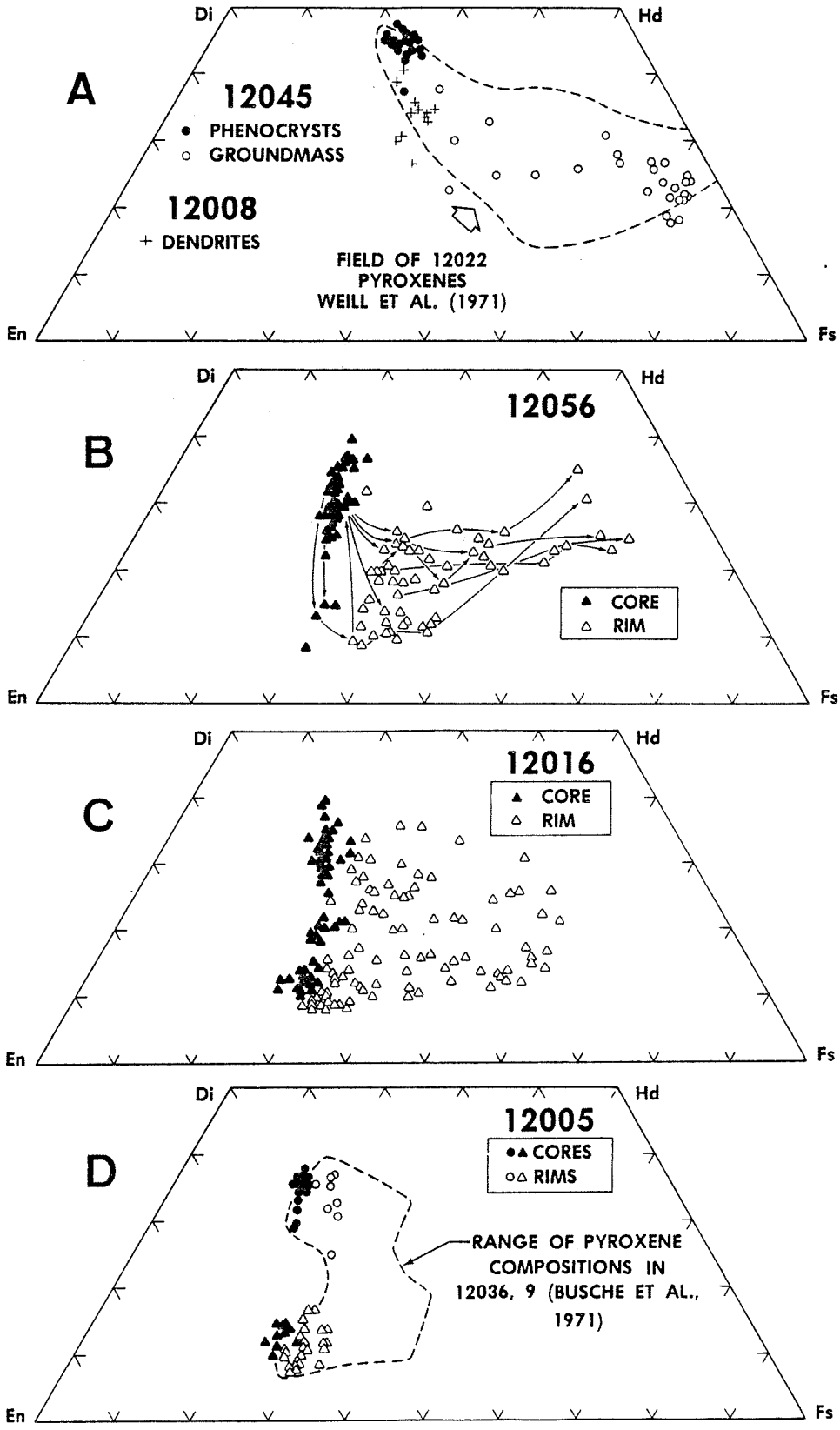
A
12045
PHENOCRYSTS
GROUNDMASS
12008
DENDRITES
FIELD OF 12022
PYROXENES
WEILL ET AL. (1971)
Di
Hd
En
Fs
B
12056
CORE
RIM
C
12016
CORE
RIM
D
12005
CORES
RIMS
RANGE OF PYROXENE
COMPOSITIONS IN
12036, 9 (BUSCHE ET AL.,
1971)

Figure 10

Figure 11

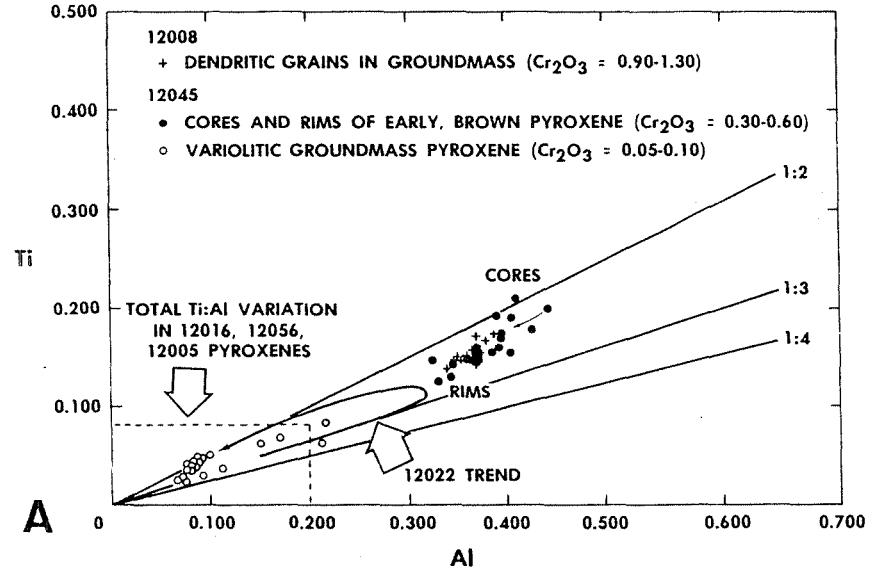
12008
+ DENDRITIC GRAINS IN GROUNDMASS (Cr_2O_3 = 0.90-1.30)
12045
• CORES AND RIMS OF EARLY, BROWN PYROXENE (Cr_2O_3 = 0.30-0.60)
○ VARIOLITIC GROUNDMASS PYROXENE (Cr_2O_3 = 0.05-0.10)
TOTAL Ti:Al VARIATION IN 12016, 12056, 12005 PYROXENES
CORES
RIMS
12022 TREND
1:2
1:3
1:4
Ti
Al
A

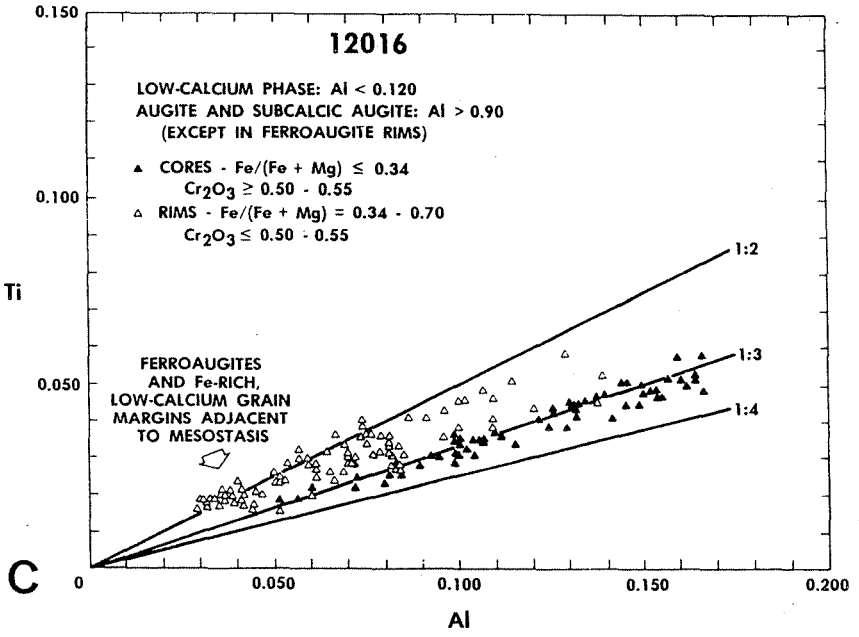
12016
LOW-CALCIUM PHASE: Al < 0.120
AUGITE AND SUBCALCIC AUGITE: Al > 0.90
(EXCEPT IN FERROAUGITE RIMS)
▲ CORES - Fe/(Fe + Mg) ≤ 0.34
Cr_2O_3 ≥ 0.50 - 0.55
△ RIMS - Fe/(Fe + Mg) = 0.34 - 0.70
Cr_2O_3 ≤ 0.50 - 0.55
FERROAUGITES AND Fe-RICH, LOW-CALCIUM GRAIN MARGINS ADJACENT TO MESOSTASIS
1:2
1:3
1:4
Ti
Al
C

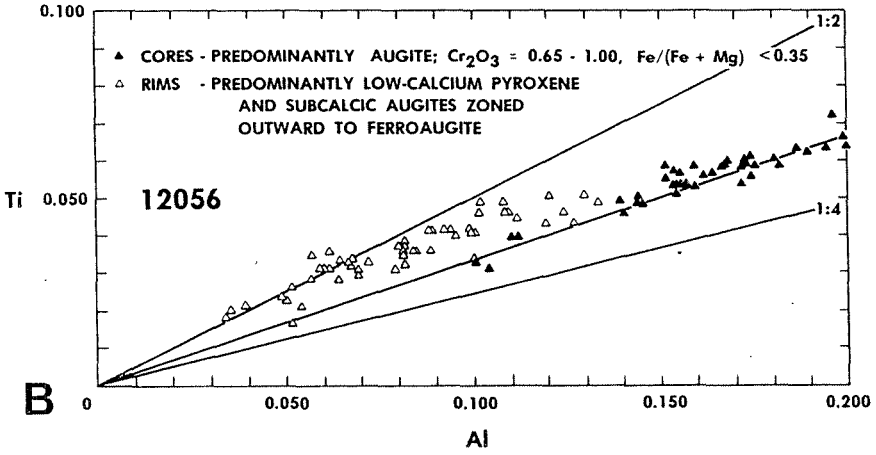
▲ CORES - PREDOMINANTLY AUGITE; Cr_2O_3 = 0.65 - 1.00, Fe/(Fe + Mg) <0.35
△ RIMS - PREDOMINANTLY LOW-CALCIUM PYROXENE AND SUBCALCIC AUGITES ZONED OUTWARD TO FERROAUGITE
12056
1:2
1:4
Ti
Al
B

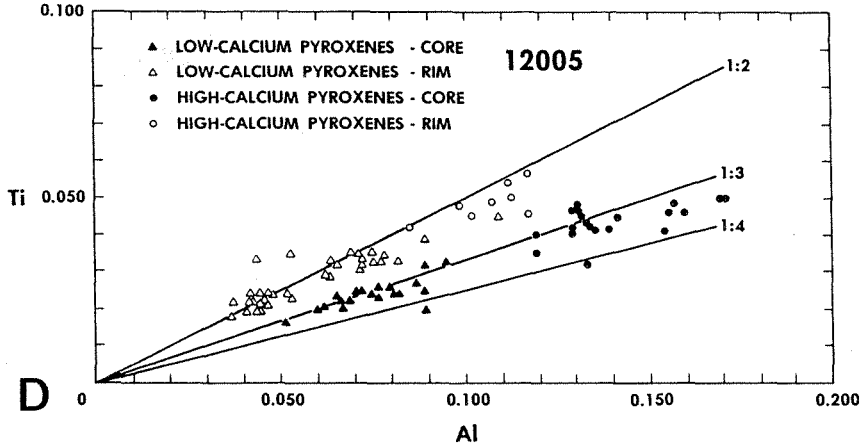
▲ LOW-CALCIUM PYROXENES - CORE
△ LOW-CALCIUM PYROXENES - RIM
• HIGH-CALCIUM PYROXENES - CORE
○ HIGH-CALCIUM PYROXENES - RIM
12005
1:2
1:3
1:4
Ti
Al
D

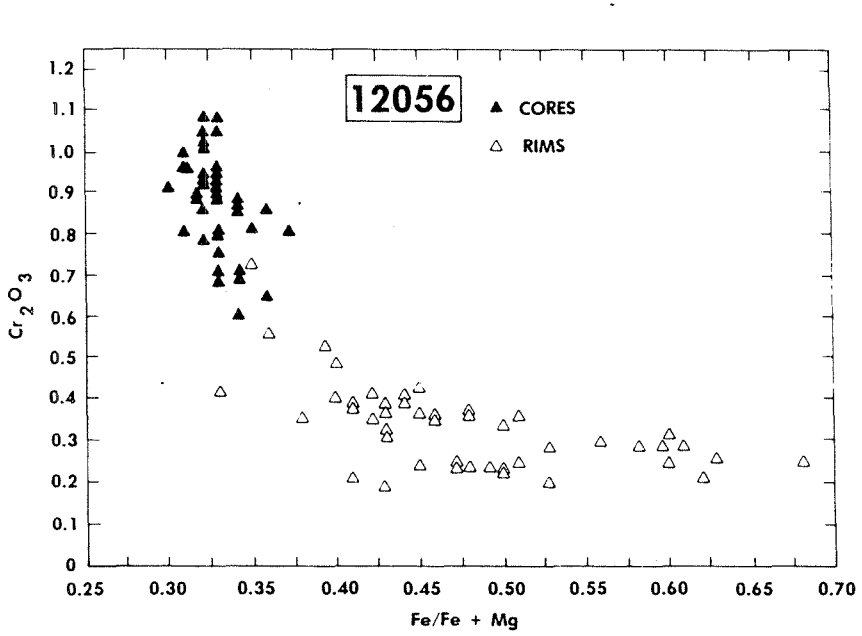
12056
▲ CORES
△ RIMS
Cr_2O_3
Fe/Fe + Mg

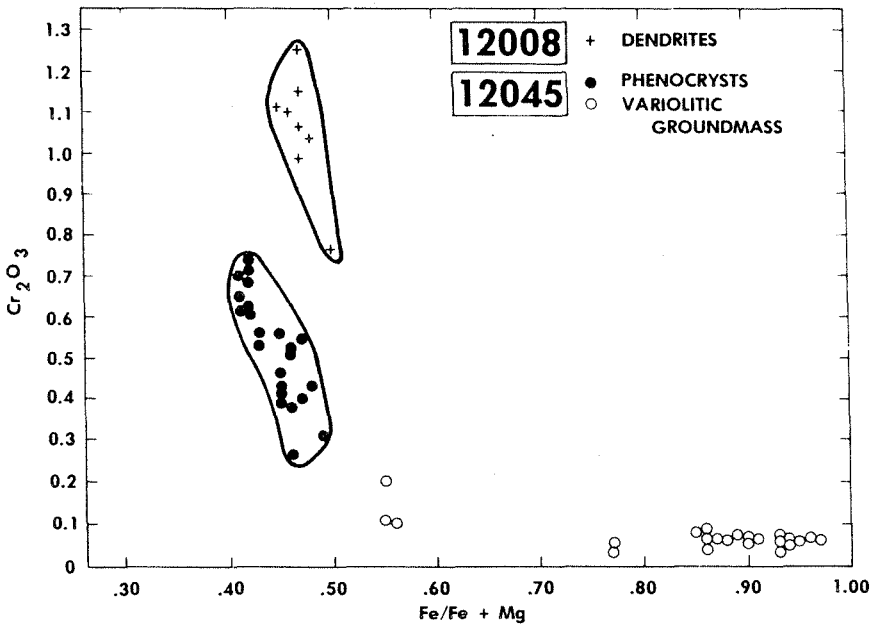
12008
12045
+ DENDRITES
● PHENOCRYSTS
○ VARIOLITIC GROUNDMASS
Cr_2O_3
Fe/Fe + Mg

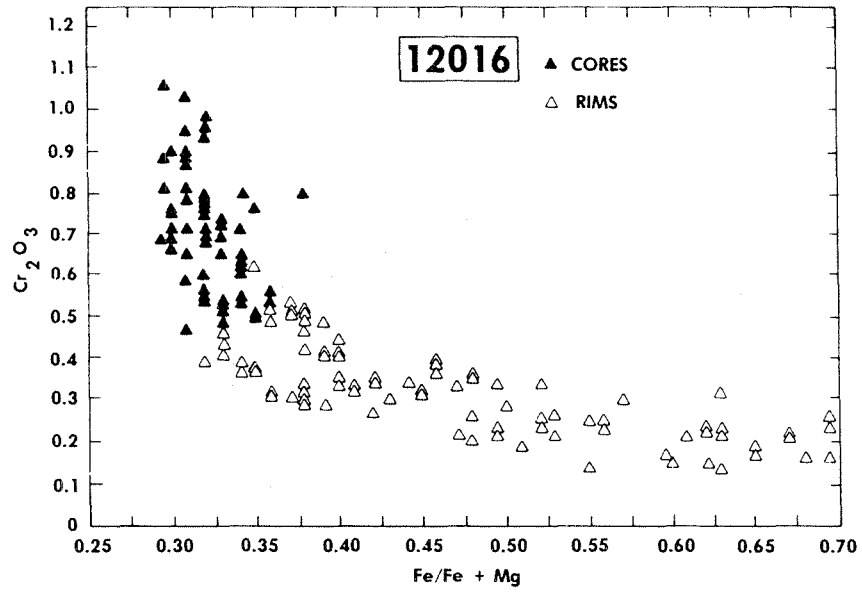
12016
▲ CORES
△ RIMS
Cr_2O_3
Fe/Fe + Mg

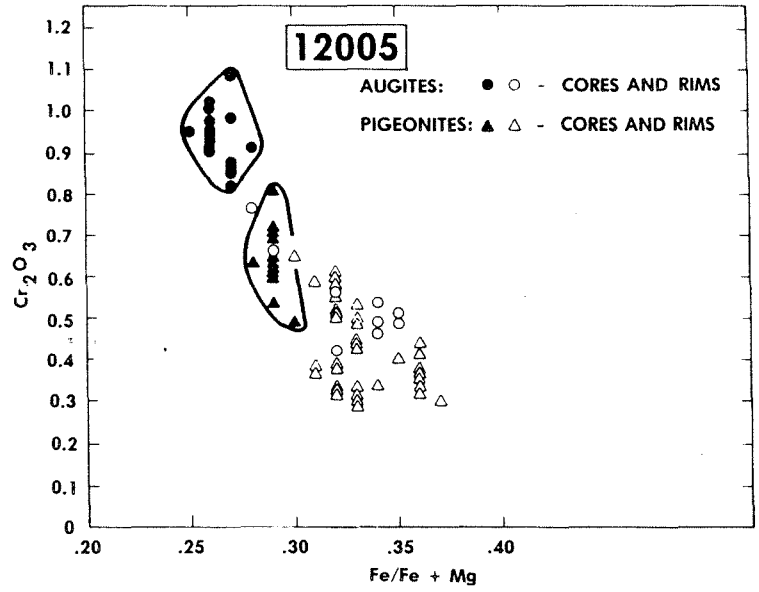
12005
AUGITES: ● ○ - CORES AND RIMS
PIGEONITES: ▲ △ - CORES AND RIMS
Cr_2O_3
Fe/Fe + Mg

Figure 12

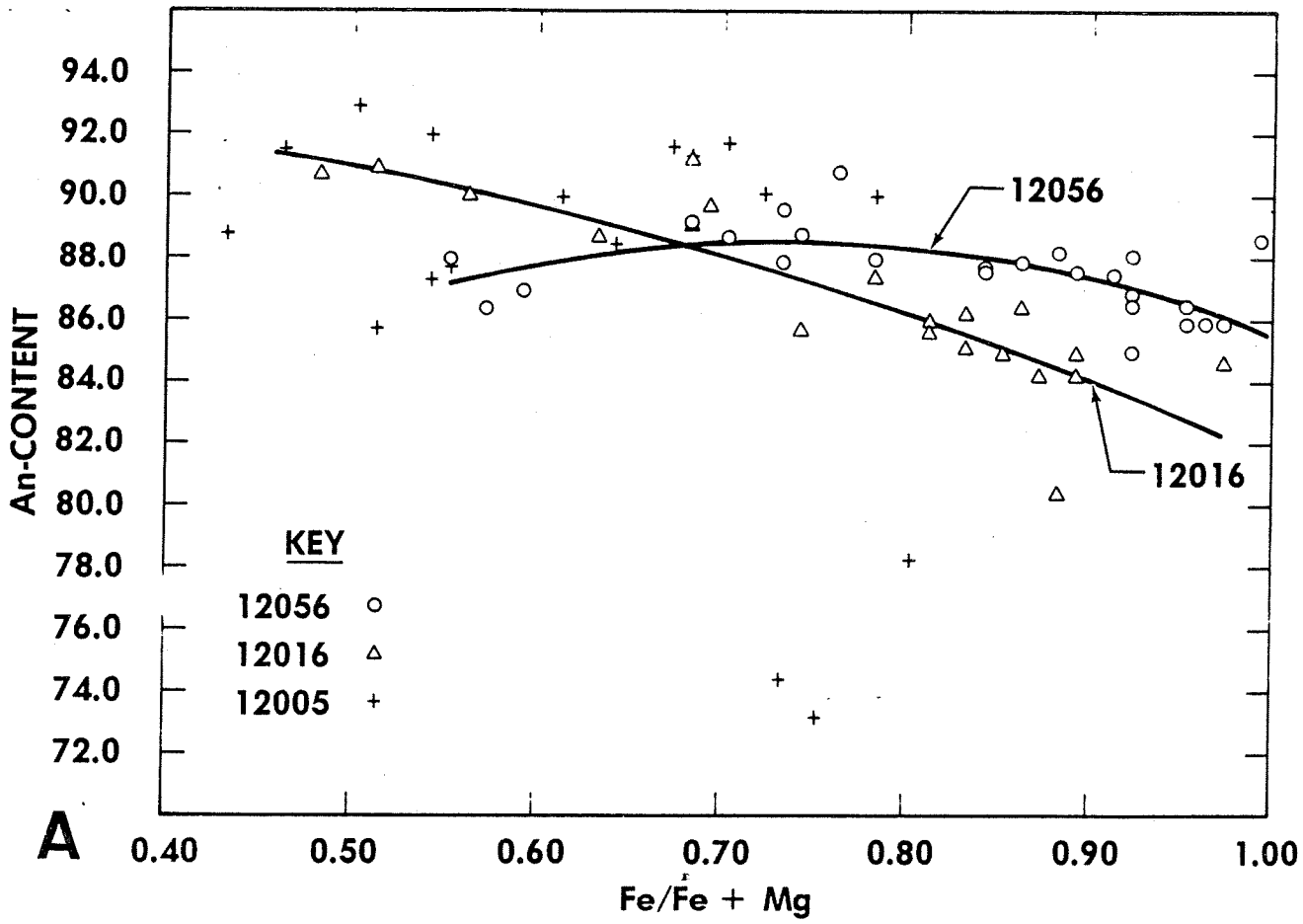
94.0
92.0
90.0
88.0
86.0
84.0
82.0
80.0
78.0
76.0
74.0
72.0
An-CONTENT
KEY
12056 ○
12016 △
12005 +
12056
12016
A
0.40
0.50
0.60
0.70
0.80
0.90
1.00
Fe/Fe + Mg

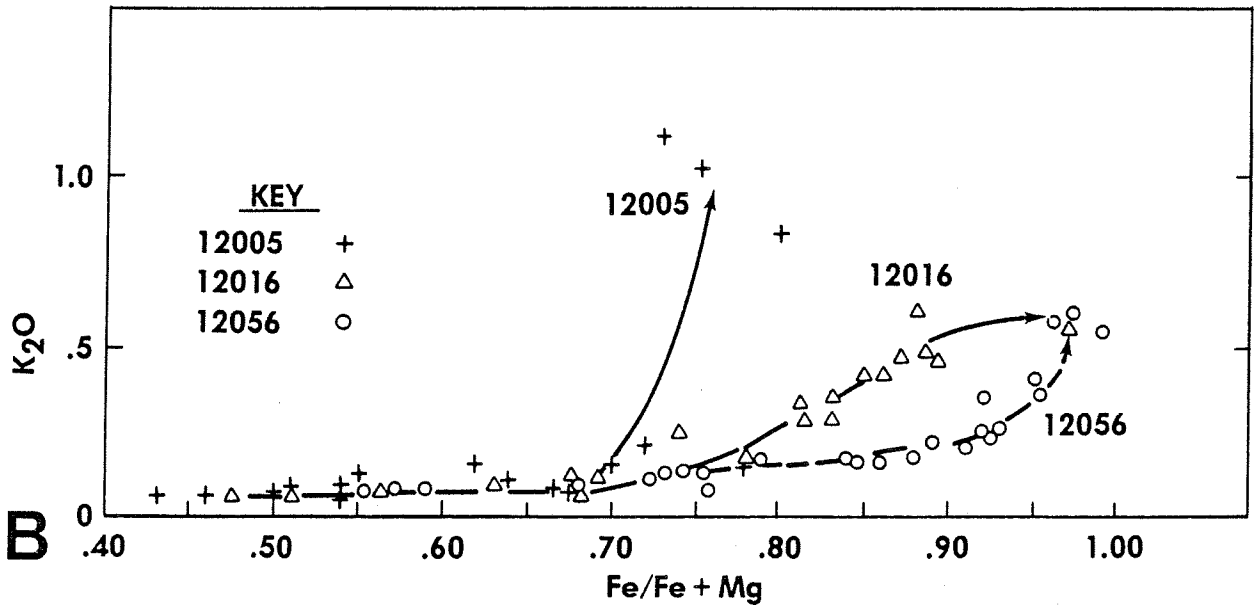
1.0
.5
0
K_2O
KEY
12005 +
12016 △
12056 ○
12005
12016
12056
B
.40
.50
.60
.70
.80
.90
1.00
Fe/Fe + Mg

Figure 13

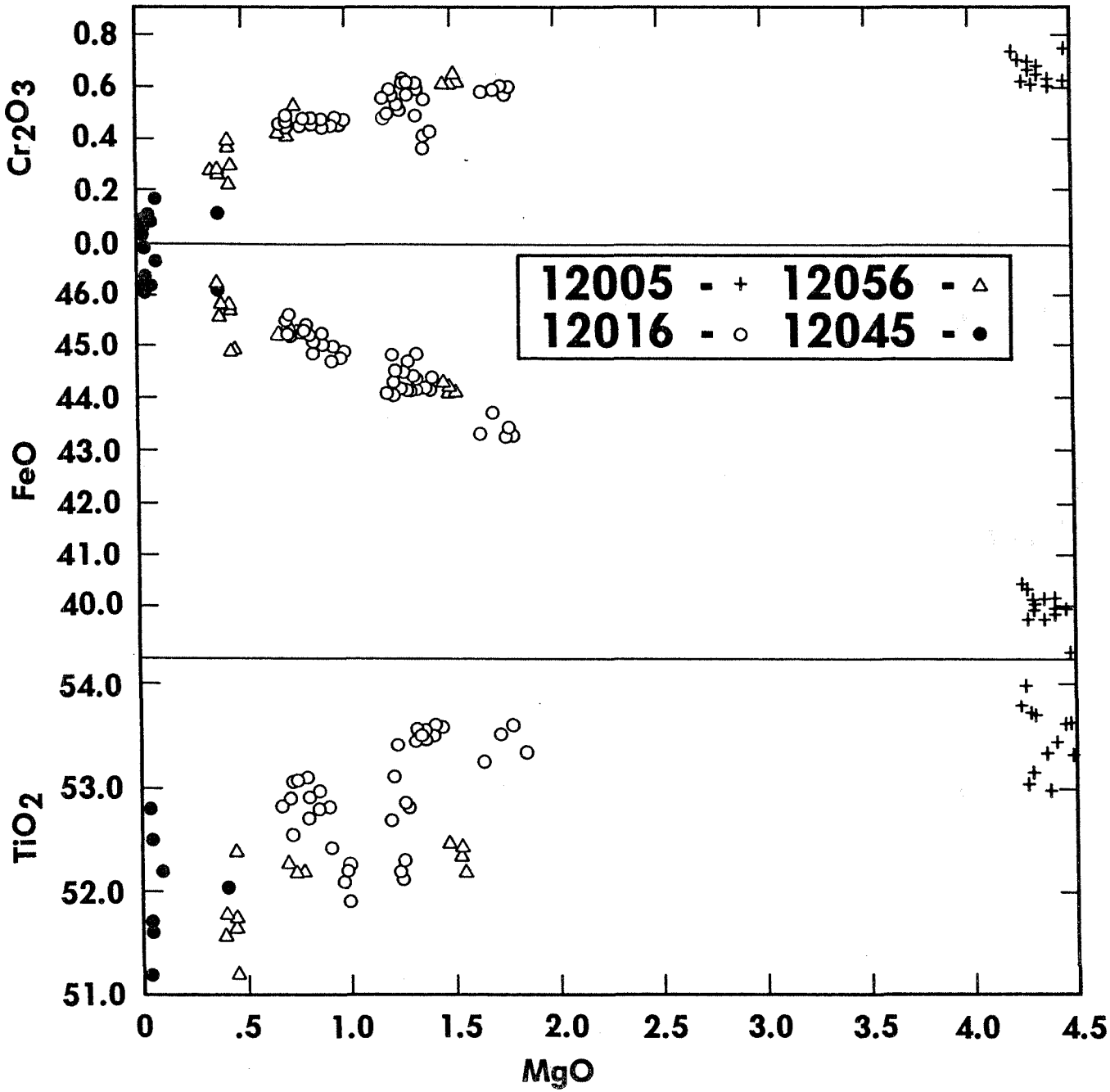
0.8
0.6
0.4
0.2
0.0
Cr2O3
46.0
45.0
44.0
43.0
42.0
41.0
40.0
FeO
54.0
53.0
52.0
51.0
TiO2
12005 - + 12056 - △
12016 - ○ 12045 - ●
0
.5
1.0
1.5
2.0
2.5
3.0
3.5
4.0
4.5
MgO

Figure 14

Figure 15